Master Sintering Curve and Its Application in Sintering of Electron

SAND2010-2158P

Christopher B. DiAntonio
Sandia National Laboratories
Materials Science and Engineering Center
Advanced Prototyping S&T
Albuquerque, New Mexico 87185-0959

Kevin G. Ewsuk
Sandia National Laboratories
Advanced Microsystem Packaging
Albuquerque, New Mexico 87185-0352

Sandia National Laboratories is a multi-program laboratory operated by Sandia Corporation, a wholly owned subsidiary of Lockheed Martin company, for the U.S. Department of Energy's National Nuclear Security Administration under contract DE-AC04-94AL85000.

ASTRACT: The ability to optimize and tailor the properties of an electroceramic is one of the most challenging aspects that an electroceramist must develop. Due to the fact that such a strong link exists between the microstructure of an electroceramic and its macroscopic electrical properties, significant efforts need to be made to control the factors and parameters that influence the characteristics of the microstructure. This chapter discusses the construction, utilization, and implementation of master sintering curves as specifically applied to electroceramics. The findings presented here demonstrate that a systematic approach to design, predict and control sintering of electroceramic systems is possible through the implementation of the master sintering curve.

KEY WORDS: master sintering curve, electroceramic, sintering, densification,

INTRODUCTION TO ELECTROCERAMICS

For many thousands of years ceramics have been used by people for a wide variety of applications. Archaeological sites in numerous areas have unearthed some of the oldest artifacts that reveal pottery was being used not only for everyday things, ex. the storage of food, but for use in the communication of information, ex. correspondence on fired clay tablets. The word 'ceramic', derived from the Greek word, *keramos*, for potter's clay or ware made from clay and fired, is based on clay and other siliceous minerals that are fired around 1000^{o}C. The meaning of the word 'ceramic' though has broadened significantly with the evolution of "pottery" to what are typically referred to as "advanced ceramics". It now tends to describe, '….solid articles which have as their essential component, and are composed in large part of, inorganic non-metallic materials'[1], although this description has also become quite limited, as amorphous materials, metallics, organics and single crystals are important components of many polycrystalline, inorganic, non-metallic and multiphase ceramics. Thus in a broad sense, a ceramic is typically defined as a polycrystalline aggregate of particles which are typically consolidated and fused into a material through the sintering process. The parameters involved in sintering a ceramic are often controlled to eliminate porosity introduced from the forming process used to make a 'green' body. It is a feature of ceramic processing that careful control is used in sintering so that, although significant linear dimensional shrinkage may be realized, the overall shape remains substantially unchanged unless by design. In the case of pottery or porcelain, phases are added that result in a liquid phase that sinters the aggregate particles together. As a property of many siliceous materials, their stability when exposed to extremes of weather and the high electrical resistivity led to the first use of ceramics in the electrical industry and the eventual development of electroceramics. Thus the methods developed for pottery were refined for the production of insulating bodies, for use in carrying and isolating electrical conductors, leading to applications in power lines, cores bearing wire wound resistors, electrical fire elements, etc.[2]

Since the turn of the 20th century ceramics have come to play an increasingly significant and important role in the electronics circuit and systems research, development and industry. The applications of ceramics in the electronics industry or 'electroceramics' can be broadly divided into two groups:

1. Materials for interconnection and packaging for semiconductor circuits
2. Functional or active electroceramics, discrete components performing a function – ex: capacitors, sensors, etc.

The first half of the 20th century was dominated by ceramics used for electrical applications based on their characteristic high degree of chemical stability and high resistivity. It also became evident with time that the possible range of properties for ceramic based electronic materials was extremely wide, as depicted in Table I.

Table I. Listing of electroceramic materials, use, approximate introduction timeframe, characteristics of interest, and applications.

MATERIAL / USE / INTRODUCTION TIMEFRAME	CHARACTERISTICS OF INTEREST	APPLICATION
Magnetite, 'lodestone' (Early 20th century)	electrical conductivity , magnetic properties, chemical inertness	Anode in the extraction of halogens from nitrates
Lanthanide oxide doped zirconia (Early 20th century)	High temperature with applied current	Nernst filament, effective source of white light
Fast-ion conductors (Early 20th century)	electrical conductivity through ion transport	Fuel cells, batteries, sensors
Ferrites (1910s), nickel-zinc and manganese zinc ferrites	high resistivity and low susceptibility to eddy currents	Choke and transformer core materials (frequencies up to and beyond 1 MHz)
Barium Ferrite, magnetic ceramic powders, garnet type structure (1930s)	ferromagnetic	permanent magnets, recording tapes, computer memory, toroids, microwave technology
Conductive ceramics (1920s)	conductive	silicon carbide heating elements
Negative temperature coefficients of resistivity ceramics (1920s)	resistivity as a function of temperature	temperature indicators
Porous ceramics, numerous compositions (1920s)	resistivity as a function of local atmosphere (moisture content and oxidation potential)	Detectors for toxic or flammable components
Dielectrics (1930s), multilayer structures, low-temperature co-fired ceramics	relative permittivity, low sintering temperature, co-sintering	Capacitors, electronics packaging, substrates
Piezoceramics, lead zirconate-titanate composition family	ferroelectricity, piezoelectricity, electrostriction, pyroelectricity, electro-optic behavior	Actuators, sensors, transducers, transformers, sonar, ultrasonics, infrared detectors,
High positive temperature coefficient resistors (PTC), doped Barium Titanate	resistivity as a function of temperature	thermostatic heaters, current controllers, degaussing devices, fuel-level indicators
Superconductors, Yttrium, Barium, Copper Oxide (YBCO)	superconductivity at high transition temperatures	electrical power distribution, permanent magnets
Porous ceramics, numerous compositions (1920s)	resistivity as a function of local atmosphere (moisture content and oxidation potential)	Detectors for toxic or flammable components
Varistors, silicon carbide and zinc oxide based ceramics (1950s)	unique and sensitive behavior of the electrical resistivity to the applied electrical field strength	Transient electrical surge suppression, Spark suppression at relay contacts
Glass-ceramics (1950s)	Electrical resistivity, thermal expansion, dimensional stability	Electrical insulators, electronic packaging technology

As one of the largest industry based areas of the ceramics field, 'Advanced Ceramics' as they are categorized and in which the electroceramics industry is typically considered a sub-category, continues to penetrate numerous applications based on their favorable performance characteristics, such as capacitors, cutting tools, membranes and orthopedic joint implants. Accounting for nearly half the advanced ceramics market demand in recent years, the use of advanced ceramics is highly dependent on the health of the electronic components and electrical equipment industries. Table II provides a short list of the applications of these advanced electroceramic systems as classified by the applied electronic function.

Table II. Application of advanced electroceramics as classified by the applied electronic function.

Electroceramic Materials	Application
Insulation – Al_2O_3, BeO, MgO	Integrated circuit, wiring, resistor, and electronics interconnection substrates, packaging, etc.
Ferroelectrics – $BaTiO_3$, $SrTiO_3$	Ceramic capacitors
Piezoelectrics – PZT, PLZT	Transducers, ultrasonic devices, oscillators, filters, spark generators, etc.
Semiconductors – $BaTiO_3$, SiC, ZnO-Bi_2O_3, V_2O_5, transition metal oxides	Negative temperature coefficient thermistors – temperature sensors and compensation, etc. Positive temperature coefficient thermistors – heater elements, switches, temperature compensation, etc. Critical temperature resistor thermistors – heat sensor elements Thick-film sensors – infrared sensors Varistors – noise suppression, surge current absorber, lightning arrestors, etc. Sintered CdS – solar cells SiC heater elements
Ionic conductors – β-Al_2O_3, ZrO_2	Solid electrolytes, oxygen sensors, pH meters, fuel cells

The United States electronic components industry is projected to remain sluggish, as Asia tends to dominate this area. However growth opportunities still exist due to materials substitution as ceramics gain use over alternatives. For example, permanent magnets and capacitors will benefit from an increase in the production of small, economical and energy efficient automobiles. Unreinforced ceramics cast directly into final form, or 'monolithic ceramics', represent the largest and best-established segment of the advanced ceramics industry. By far the dominant monolithic product, accounting for half of the total monolithic ceramics demand recently are ceramics for electrical equipment and electronic components.

Although produced from numerous materials, these advanced ceramics are typically manufactured from materials with very high purity levels and are sintered under strictly controlled profiles and conditions, unlike the more traditional ceramic products such as flooring, wall tile, pottery, china, refractory brick, etc. This results in specifically tailored microscopic/macroscopic properties, ex. conductivity, resistivity, permittivity, ferroelectricity, etc., which are critical to the proper performance of the component in application. The final macroscopic properties therefore are intimately tied to the chemical composition of the material (based on the intrinsic properties), atomic structure, ceramic fabrication techniques, and microstructure of the polycrystalline ceramic, as illustrated in Figure #1. Presently an enormous factor in the industry is associated with rising production costs, as seen in energy and machining costs. These costs could be addressed and possibly even reduced through more exact product forming by employing near-net shape techniques and improved sintering control, prediction and modeling.

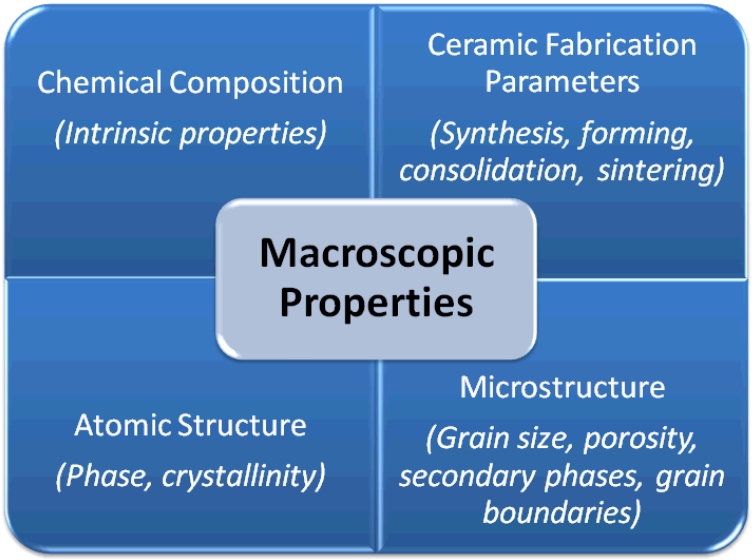

Figure #1. Illustration depicting the intimate tie of the chemical composition, atomic structure, ceramic fabrication parameters, and microstructure to the macroscopic properties of a material.

SINTERING AND DENSIFICATION OF ELECTROCERAMICS

Ceramics can densified by solid-state[3-6], liquid-phase[7], and viscous[8] sintering. Overall, the reduction in surface energy as the free surfaces of initially individual and discrete particles coalesce is the major 'driving force' for densification mechanisms in a polycrystalline ceramic material. Specifically, polycrystalline ceramics sinter as a result of the thermodynamic driving force to minimize the Gibbs' free energy, G, of a system[9-13], including minimizing the volume, interfacial, and surface energy in the system. This reduction in energy is accomplished by atomic level diffusion processes. These processes result in either densification of the ceramic body (internal grain matter is transported to the pores), coarsening of the microstructure (rearrangement of matter from various locations on pore surfaces with none to minimal decrease in pore volume), or a complex combination of all mechanisms. The sintering process encompasses permanent chemical and physical changes in a ceramic body that are occurring in harmony with changes in the porosity and density. Excess free energy, in a consolidated powder body, is primarily present in the form of the surface or interfacial energy (i.e., liquid-vapor and/or solid-vapor interfaces) associated with porosity. Atoms migrate to thermodynamically more stable positions under the influence of elevated temperature and/or pressure during sintering. The chemical potential difference that exists between surfaces of dissimilar curvature within the system is what essentially drives material transport. As viewed from the center of a particle out, for a particulate system, atoms or ions move from higher energy convex particle surfaces to lower energy concave particle surfaces to decrease the curvature and chemical potential gradients in the system. The transport of material can occur by solid-state (material transfer by solid state diffusion), liquid-phase (material transfer by solubility and precipitation in the liquid phase), and/or vapor-phase (material transfer by vapor transport between particles) mechanisms. This transport commonly occurs as ions diffuse through the volume, along grain boundaries (i.e., particle-particle intersections), and on particle surfaces, as depicted in the simplified 'two-sphere model' illustration in Figure #2. Material transport occurs through the process of diffusion, the movement of atoms/ions, sometimes referred to as atom jump. Diffusion can occur along a number of paths including, but not limited to, grain boundaries or through the grain itself (lattice diffusion). Additionally, ions can vaporize from particle surfaces and subsequently re-condense onto more energetically favorable particle surfaces (i.e., evaporation-condensation). In general, when material transport occurs in such a manner that allows particle centers to approach during sintering a ceramic body will undergo volume contraction and densify (volume and grain boundary material transport mechanisms can result in densification). If the active and dominant material transport mechanisms only change the geometry of the system without densification then only coarsening of the microstructure will result. Coarsening can occur when material is transported by volume diffusion, surface diffusion and/or evaporation/condensation. The most prevalent form of coarsening during the sintering process tends to be grain growth.

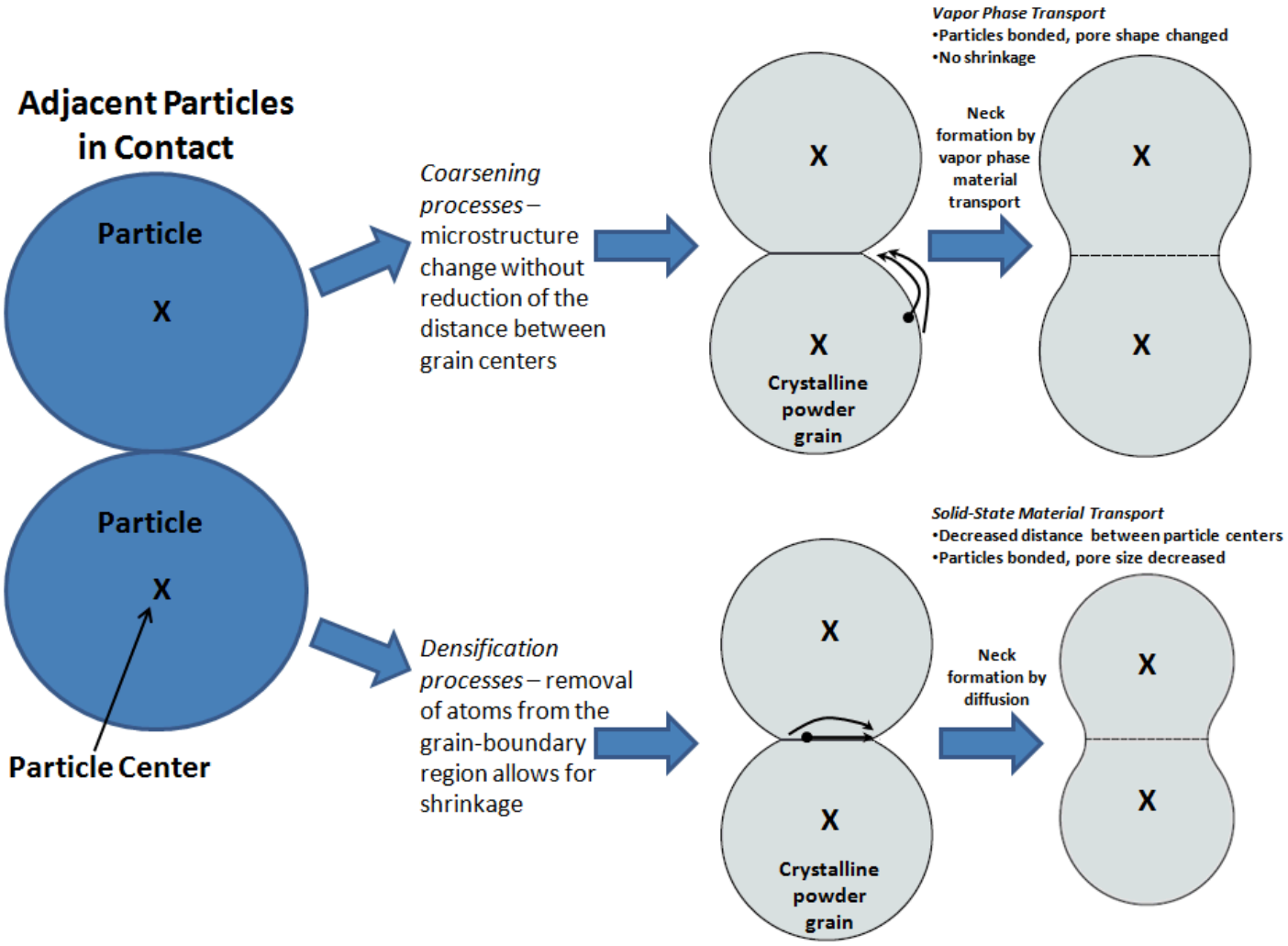

Figure #2. Schematic representation of a generic 'two-sphere' model showing the simplified distinction between coarsening (non-densifying) and densification processes that result from atom movement (diffusion) during ceramic sintering.

Densification and Microstructure Development

It is in the sintering stage of the overall ceramic fabrication route that the ceramic body develops the desired microstructure. Interparticle pore shrinkage, grain boundary formation, a decrease in the total volume of the system through densification and an increase in the average size of the particles that make up the ceramic system through grain growth is how, from the aspect of the microstructure, material transport manifests itself during sintering. As sintering progresses, the surface area and free energy of the system decrease as interparticle contacts are subdued and the overall curvature in the system decreases.

Three basic stages have been defined for the 'ideal' sintering process; initial, intermediate, and final stage sintering.[3,6] In the initial stage, necks form between adjacent particles as material is transported from convex particle surfaces to the pore-grain boundary intersection. The grain boundaries grow to create a three-dimensional array of approximately cylindrical, interconnected and continuous pore channels at three grain junctions. The onset of the intermediate stage of sintering can then be defined when the diameter of these pore channels decreases. The channels eventually pinch off, due to Rayleigh instability (critical 'cylinder' length to diameter ratio), to approximately spherical and isolated (closed) pores at four grain junctions in the

ceramic microstructure matrix. The final stage of sintering is marked with the radial shrinkage of these closed pores and the growth of larger grains at the expense of smaller ones.

Depending on the complexity of the starting materials, the changes occurring during sintering may be fairly complex in nature. The complex nature of the process has led to its analysis through a combination of theoretical analyses in terms of modeling (in many cases idealized modeling) combined with experimental investigations. The understanding of the sintering process/mechanisms therefore has matured considerably in the last half century. The major conceptual advances have originated, to a significant extent, from the advances in researchers ability to observe, characterize and quantify the sintering and densification mechanism(s) involved in the process.

For the majority of electroceramic materials sintering is achieved either by solid state or liquid phase sintering mechanism(s), at least in the absence of an appreciable amorphous or glassy phase. A major constituent in tableware and electrical porcelain is the formation of a glassy phase that mainly develops from the presence of fluxes (feldspathic minerals). The glassy phase forms and wets the surfaces of the solid phase and a large fraction of the porosity is filled with glass as the surface tension forces pull the mass of particles together. In almost all cases some of the initial porosity gets trapped in the microstructure as the gas cannot escape quickly enough through the vitreous phase. The glassy phase also tends to form a continuous network in the microstructure, resulting in modified electrical properties. This manifests itself in a tailored dielectric loss based on the application and intended use, so that electrical porcelain is used for adequate electrical insulation as the major requirement. In the absence of this glassy phase densification can be achieved by solid state or liquid phase sintering mechanism(s) or some complicated combination of these mechanisms.

Solid State Sintering

For solid state sintering to initiate, the ions composing the ceramic must have sufficient mobility in the microstructure. This is typically not achieved until the temperature of the ceramic is greater than approximately 80% of the melting temperature. In the early stages of solid state sintering the microstructure undergoes significant changes. One of the dominant diffusion mechanisms in this early stage can be attributed to the surface diffusion of ions from convex surfaces, higher energy state, to the concavities at particle contact points, lower energy state. This mechanism however does not contribute to any appreciable densification as the process of mass transport from grains to pores is necessary, a process which commonly occurs by vacancy diffusion from regions close to the surface of a pore. The vacancy concentration in these regions of the microstructure is high relative to the equilibrium concentration in the bulk of the ceramic. The grain boundaries act as vacancy sinks by virtue of their intrinsic disorder.

Overall, densification occurring by solid-state diffusion controlled material transport refers to the process of ‘solid-state’ sintering. As higher energy solid-vapor interfaces, porosity, are replaced by lower energy solid-solid interfaces (grain boundaries) densification can occur. The densification is driven by the change in free energy associated with the elimination of this porosity. Following the elimination of pore surfaces and completion of densification, the free energy of the system can be further reduced by reducing the amount of high-energy solid-solid interfacial area through grain growth. The grain growth is driven by the change in free energy associated with the elimination of particle-particle interfaces. Therefore densification occurs via the reduction in size of thermodynamically unstable porosity. It is however the thermodynamics and/or the kinetics that limit the shrinkage of pores trapped within grains, intra-granular porosity, and pores larger than a ‘critical’ size.[14-16]

Liquid-Phase Sintering

In liquid phase sintering, conditions of temperature and composition are chosen so that a quantity of liquid, usually on the order of a few volume percent or less, is formed between the grains of the ceramic. Traditional liquid-phase sintering involves heating and melting crystalline solids to form a eutectic liquid during sintering.[7] Ion mobility is assisted by the formation of small quantities of the liquid. It is important for liquid phase sintering that the crystalline phase has a limited solubility in this liquid to avoid any dissolution processes. In this case a 'solution precipitation' process, where ions dissolve at high energy sites and precipitate at lower energy sites, produces mass transport (one of the most common liquid phase sintered electroceramic components is the alumino-silicate based compositions used in low temperature co-fired ceramics). Transport of dissolved grain material through the liquid allows closer packing of the grains and densification of the material as the grains are reshaped. As the material cools the liquid crystallizes or forms a glass and can yield a dense solid ceramic body. Therefore, for liquid-phase sintering, the requirements include, that the liquid wets the solid particles, there is sufficient liquid present, and the solid is soluble in the liquid. As the temperature is increased above the eutectic temperature there is an increase in the concentration of the liquid and the solubility of the solid in the liquid or an increase in the reactivity. Overall, if it is energetically favorable to replace the liquid-vapor, solid-solid, and solid-vapor interfaces during sintering then densification will proceed.

The process of densification during liquid-phase sintering can be described in a series of stages. Initially the liquid forms at particle intersections and begins to redistribute itself through the ceramic matrix due to the influence of capillary action. Particle rearrangement, typically resulting in improved particle packing, occurs due to shear stresses that have developed from the capillary pressure imbalance on the individual particles (each having a particular size and morphology) and contributes to the initial stage densification. The microstructure continues to mature into an intermediate stage where solution-precipitation controls the densification. Material located at higher energy convex particle surfaces starts to dissolve and can now migrate to lower energy pore surfaces where it precipitates out of solution. It is at this point where individual grains can actually change shape to fill in void space (porosity). This process is often referred to as 'grain accommodation'. A rigid three-dimensional skeletal structure starts to form and densification continues by solution-precipitation. When closed pores are formed the transition to the final stage of liquid phase begins and, as with solid-state sintering, is characterized by the shrinkage of isolated pores and grain growth.

Due to the fact that such a strong link exists between the microstructure of a ceramic and its macroscopic electrical properties, significant efforts need to be made to control the factors that influence the characteristics of the microstructure, including the grain size distribution, grain boundary characteristics, porosity, etc. Optimized conditions, initial particle sizes, tailored sintering schedules, and specific chemical compositions need to be determined based on the macroscopic property needs for a particular application or use. In some cases the differences in grain growth and densification kinetics could be exploited to produce a desired and optimized macroscopic property. It should also be mentioned that not in all cases involving the sintering of electroceramics is it always possible to obtain a minimal porosity body by 'pressureless sintering', sintering at atmospheric pressure, as just discussed. In some situations an optimized microstructure may require the complete elimination of porosity and the maintenance of a discrete grain size or grain size distribution. Hot pressing, hot forging, spark plasma (field assisted) sintering and/or isostatic hot pressing is typically employed as a sintering technique to overcome these problems. These techniques provide more control over the sintering temperature and can minimize crystal growth as the pressure and/or applied electric field now provides the major part of the driving force to eliminate porosity and densify the microstructure as desired.

MASTER SINTERING CURVE AS APPLIED TO ELECTRONIC CERAMICS

The ability to optimize and tailor the properties of an electroceramic is one of the most challenging aspects that an electroceramist must develop. This includes having the understanding of at least the basic science of a range of properties, including but not limited to the conductive, dielectric, optical, piezoelectric, and magnetic properties and how they are intimately tied to the overall science of the ceramic. The science though can be exploited to optimize the desired properties through the design of the material composition and the tuning of the microstructure and texture. The additional objective of a significantly reduced sintering temperature and minimization of the efforts for ceramic manufacturing for the final component often make property optimization extremely difficult. Conventional microcrystalline powders present problems due to agglomeration, surface contamination, undesired grain coarsening, exaggerated grain growth, etc., that make reproducible ceramic processing of homogenous materials, that retain the highly desirable features after sintering, a challenge. The cost effective manufacture of reliable ceramic components is critical for advanced ceramic component manufacturing and is typically manifested in robust and reproducible ceramic processing. The processes used to manufacture ceramic components has historically been developed from empirical engineering, this however alone cannot provide the necessary fundamental understanding for material processing. The integration of a fundamental scientific understanding into a science-based processing technology that can be applied to more fully understand ceramic powder processing and sintering is one approach.[17-24] The driving force for densification, microstructure evolution, mechanisms and paths for material transport during sintering[6,25-27] are reasonably well understood (Note: the provided references are in no way exhaustive of the numerous literature sources available but are only intended to provide a starting point for exploration into the enormous subject of the sintering of ceramics, the additional chapters provided in this book also provide extensive information on these topics). The practical application of this fundamental sintering science and the link to a set of desired properties though remains a challenge. Over the years researchers have developed and used processing and sintering maps to design and interpret sintering experiments in an effort to gain a better understanding of how specific thermal profiles affect the sintering behavior and resultant ceramic microstructure.[28-34] These maps aid in simplifying the analysis of sintering results and have the potential of enabling practical application of the fundamental science of sintering theory for ceramic manufacturing. Recently another promising and practical approach to predict, control and tailor sintering has been introduced and is based on the concept of a master sintering curve (MSC).[35-45]

The MSC provides a characteristic measure of the densification of a material, within the boundary conditions of a specific density range, as determined through experimentation. It is an empirical curve and unique for a given material processed in a specific manner. By constructing an MSC for a given system the density and densification rates of a ceramic body can be predicted. The construction of the curve requires a few basic dilatometric sintering experiments, providing the necessary sintering behavior to allow predictions for almost any combination of sintering time and temperature, within the boundary conditions. Comparisons of the predicted, experimentally measured, and modeled sintered densities of numerous ceramic systems has provided overwhelming verification of the predictive power of the master sintering curve concept.[44,46,47] Although originally developed and demonstrated for traditional microcrystalline solid-state sintering ceramic systems, with isotropic sintering behavior, the concept of the master sintering curve has been extended to encompass systems exhibiting anisotropic, liquid phase, viscous phase and nanocrystalline sintering behavior.[47]

For the constructing and implementation of a master sintering curve the parameters in the sintering rate equation that governs it are separated, with terms related to the development of the microstructure and terms related to the temperature realized by the body, to opposite sides of the equation. The two sides of the equation are then related to each other experimentally. In most cases, for ceramic powder systems and ceramic processing and forming techniques, the geometric parameters of microstructure are independent from the thermal sintering path, making this generalization possible and coherent. Although a general

concept, the formulation and construction of a MSC is derived from the combined stage sintering model.[27] The instantaneous linear shrinkage rate and equivalent isotropic densification rate as described by this model is given as:

$$-\frac{dL}{Ldt}=\frac{d\rho}{3\rho dt}=\frac{\gamma\Omega_a}{k_BT}\left(\frac{\delta D_b\Gamma_b}{G^4}+\frac{D_v\Gamma_v}{G^3}\right) \quad (1)$$

ρ = density of the ceramic body (g/cm3)
γ = specific surface free energy
Ω_a = atomic volume
k_B = Boltzmann constant
G = mean grain diameter
δ = grain boundary thickness (thickness of the region of enhanced diffusion at the grain boundary)
D_b = grain boundary diffusion coefficient
D_v = volume diffusion coefficient

Γ_b = geometric factor for grain boundary diffusion = $\dfrac{\alpha C_{\mathrm{k}}\, C_{\mathrm{b}}}{C_{\lambda}\, C_{\mathrm{a}}\, C_{\mathrm{h}}}$ (2)

Γ_v = geometric factor for volume diffusion = $\dfrac{\alpha C_{\mathrm{k}}\, C_{\mathrm{v}}}{C_{\lambda}\, C_{\mathrm{a}}\, C_{\mathrm{h}}}$ (3)

This model extends the analysis of sintering beyond the secluded segments proposed by models that only account for individual sintering stages. Sintering models have been sought for since the earliest quantitative sintering studies were performed, with the typical objective being to gain a deeper understanding of the mechanisms involved in densification and acquire the ability to relate sintering rate to the particle characteristics, 'as-formed' ceramic body characteristics, atmosphere and thermal profile. In many cases the use of simplified geometries was used to identify sintering driving forces, mass transport paths, and geometric factors. As sintering proceeds the geometric factors continuously change and can be understood based on the DeHoff model[48], where each of these factors in equations (2) and (3) relates the mean grain diameter to a particular geometric factor for sintering, according to:

$\nabla\mu = \frac{\alpha K}{\lambda}$ = *gradient in chemical potential*

$\lambda = C_{\lambda}\, G$ = *maximum distance of diffusion*

$\mathrm{K} = -\frac{C_{\mathrm{k}}}{\mathrm{G}}$ = *curvature at the pore or neck surface*

$\delta L_b/2 = \delta G C_{\mathrm{b}}$ = *area for grain boundary diffusion*

$A_v = C_v G^2$ = *area for volume diffusion*

$S^b = C_a G^2$ = *grain boundary area at the base of the pyramid*

$h = C_h G$ = height of the pyramid

> Note: In this model each grain is considered to be an irregular polyhedron defined by the grain boundaries between the grain and its nearest neighbor, where the polyhedron comprise pyramids with a common apex at the center of the grain, the bases are defined at the grain boundaries. By extending the polyhedron into the pores the total volume of the body is included in the sum of all the polyhedral.

Thus these grouped scaling parameters, Γ, relate the instantaneous shrinkage rate to the diffusion coefficient and other material parameters and mean grain diameter. Unless significant exaggerated grain growth or excessive surface diffusion occurs during sintering these experimentally determined values are dependent on the density of the body but are independent of the thermal profile in most cases. Recognizing that both the mean grain diameter, G, and the scaling parameters, Γ, will evolve with density, and assuming that densification during sintering is a thermally activated process and controlled by an single dominant diffusion mechanism (i.e. typically grain boundary diffusion for fine grain size ceramics), it was proposed[35] that equation (1) be rearranged, integrated and simplified to:

$$\int_0^t \frac{1}{T}\exp\left(-\frac{Q}{RT}\right)dt - \frac{k}{\gamma\Omega D_o}\int_{\rho_o}^{\rho}\frac{(G(\rho))^n}{3\rho\Gamma(\rho)}d\rho \tag{4}$$

where Q is the apparent activation energy (Joules/mol), R is the gas constant, $D_o = (D_v)_o$ and n=3 for volume diffusion, $D_o = (\delta D_b)o$ and n=4 for grain boundary diffusion. The much easier determined processing parameters of sintering time and temperature are now intentionally isolated from the more difficult to measure microstructure and material property parameters. The master sintering curve equations are now derived as:

$$\theta(t, T(t)) \equiv \int_0^t \frac{1}{T}\exp\left(-\frac{Q}{RT}\right)\mathrm{d}t \tag{5}$$

$$\Phi(\rho) \equiv \frac{k}{\gamma\Omega D_o}\int_{\rho_o}^{\rho}\frac{(G(\rho))^4}{3\rho\Gamma_b(\rho)}\mathrm{d}\rho \tag{6}$$

Equations (5) and (6) are then related to one another experimentally by the instantaneous sintered density, ρ(t) and the master sintering curve can be constructed empirically from a plot of the ρ(t) for a specific sintering time and temperature as a function of log θ(t, T(t)) for the same time and temperature. A sintering process model is essentially derived from the data and it should be noted that no assumption is made about the dependence of temperature on time. Providing the boundary conditions under which the MSC was

determined are not violated the sintering characteristics can now be predicted for arbitrary temperature-time excursions.

A commonly used method for obtaining the necessary data for the construction of the master sintering curve for a particular material is to employ a dilatometer and perform a series of constant heating rate sintering experiments on the as-formed samples. The final densities of the samples are measured following the experiment and the density, at various times during the thermal profile, is calculated from the linear shrinkage data. An example of the results from this type of sintering characterization for a low temperature co-fire ceramic (LTCC) system is shown in Figure #3.

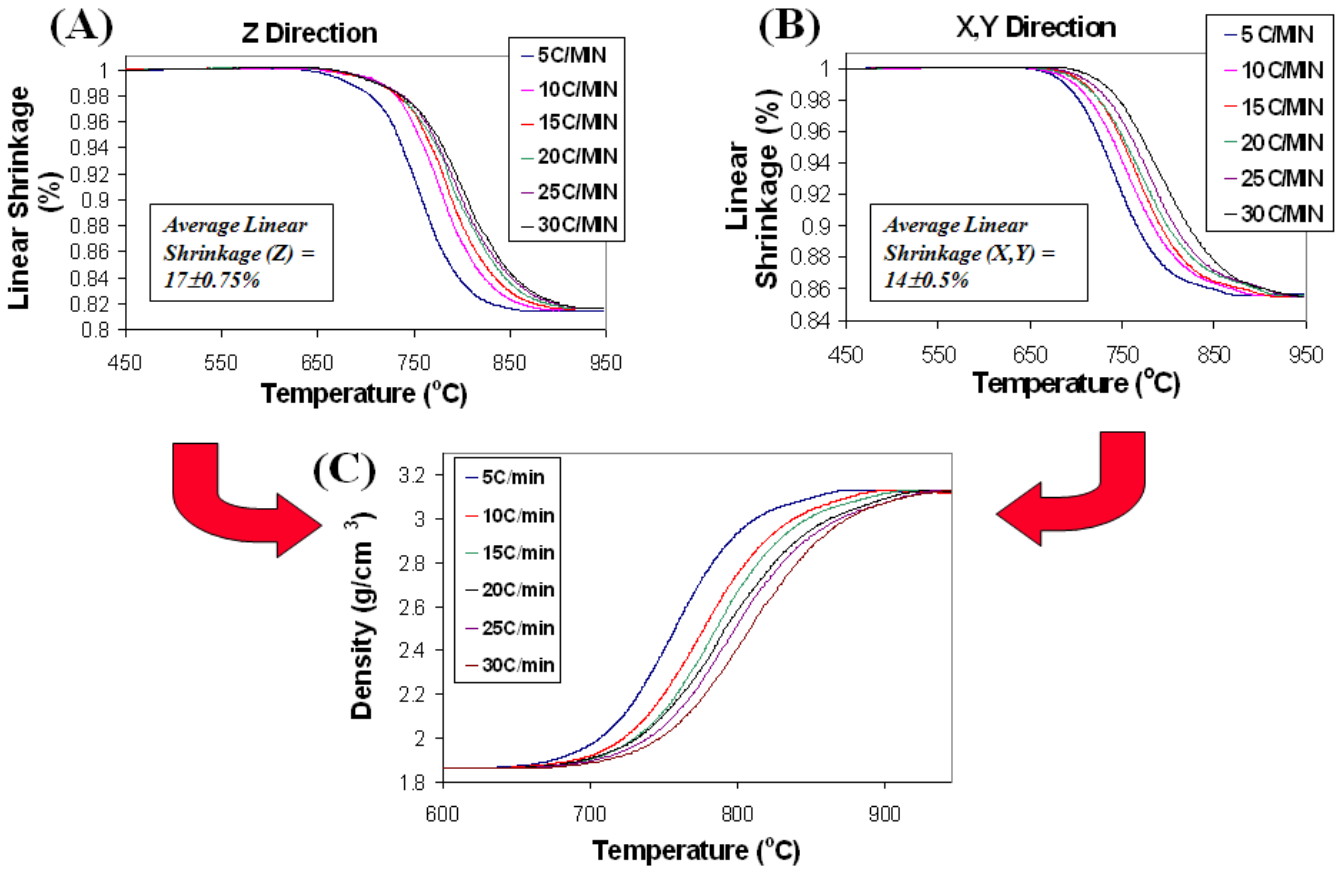

Figure #3. Linear shrinkage (%) as a function of temperature for constant heating rate experiments (5, 10, 15, 20, 25 and 30°C/min) for a Dupont low temperature co-fire dielectric tape, 951 Green Tape™, (A) Transverse to the plane direction (Z-direction), (B) In-plane direction (X,Y-direction), and the linear shrinkage results collapsed onto (C) density as a function of temperature for each heating rate.

In this case an anisotropically densifying low temperature co-fire ceramic (LTCC), Dupont low temperature co-fire dielectric tape, 951 Green Tape™, has had its sintering behavior characterized as a function of several constant heating rate experiments (5, 10, 15, 20, 25 and 30°C/min). Low temperature co-fire ceramic (LTCC) packaging technology is being used to produce advanced electronic components (e.g., for wireless communications). The ability to predict and carefully control sintering shrinkage is of critical importance in LTCC manufacturing. The goal of this study was to evaluate the master sintering curve (MSC) as a tool to predict and control LTCC sintering. Dilatometer sintering experiments were designed and completed to

characterize the anisotropic sintering behavior of the DuPont 951 Green Tape™ and the MSC was modified to account for the anisotropic sintering behavior. Due to the anistropic densification of the LTCC it was necessary to characterize both the transverse (Figure #1, A) and in-plane (Figure #1, B) linear shrinkage and then collapse these into one density trajectory as a function of temperature (Figure #1, C) plot for the material. Once this density trajectory, as a function of a few constant heating rates, was determined the master sintering curve was constructed from a computation of the master sintering curve parameter, θ, values for each data point. It is at this point that a known, assumed, or calculated value of the apparent activation energy (*Q*) is necessary. The value of the apparent activation energy for densification during sintering can be determined using several techniques: (Note: assuming valid and consistent results, each of these techniques should yield approximately equivalent values.)

1. Minimization of residuals between the constructed master sintering curve and a fit curve, residual difference between the MSC predicted values and the fit curve values (Note: the results from this technique are dependent upon the type of curve fitting function used).
    a. The dispersion is best assessed quantitatively, where each individual constant heating rate experiment is ignored and the data is lumped into a single set. A function is then fit to the data set and the mean square residual is computed from the predicted density of the MSC and the fit function at each data point. The fit curve functions can be polynomial fits, a sigmoidal curve fit, etc., each function having advantages and disadvantages based on the characteristics of the data set and the preferences of the user. The following equation provides an example for a sigmoidal curve fitting function that can be used:

$$\rho = \rho_o + a \,/\, [1 + \exp(- (\log(\theta) - \log(\theta_o)) \,/\, b))]^c \qquad (7)$$

ρ = density
ρ_o = initial density (lower asymptote)
θ = master sintering curve parameter
θ_o = value of at the point of inflection of the fit curve
a = difference between the upper and lower asymptotes
b = curve shape parameter
c = curve shape parameter

2. Minimization of residuals from the empirical construction of the MSC – mean square residual from the difference between the constant heating rate experiments for each θ value. An example of the output plot and mean residual squares equation from this minimization technique, for the LTCC sintering analysis, is show in Figure #4.

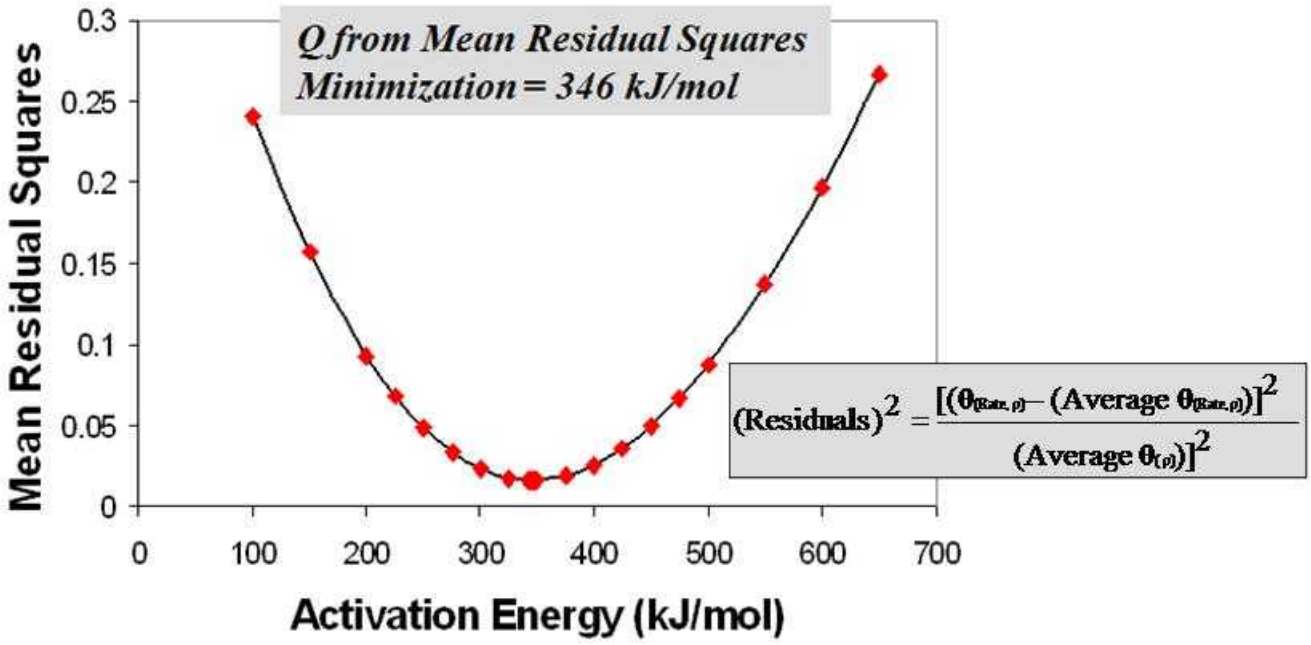

Figure #4. Example of the output plot and mean residual squares equation from the minimization of residuals from the empirical construction of the master sintering curve, difference between the constant heating rate experiments for each θ value, for the Dupont low temperature co-fire dielectric tape, 951 Green Tape™.

3. Experimentally determined using the time, temperature, and density data from the constant heating rate sintering experiments, and the following expression[49,50]:

$$\ln\left(T\,\frac{dT}{dt}\frac{d\rho}{dT}\right) = -\frac{Q}{RT} + \ln[f(\rho)] + \ln A - n\ln dG \tag{8}$$

where T is the absolute temperature, t is time, R is the gas constant, $f(\rho)$ is a function of density, G is the grain size (grain diameter), n is the grain size power law exponent (depends on whether the densification rate is controlled by volume (lattice) diffusion, $n = 3$, or by grain-boundary diffusion, $n = 4$) and A is a material parameter (constant) that is insensitive to G, T and ρ. The formulation was derived from a general sintering rate equation that separates the temperature dependent, grain size dependent, and density dependent quantities:

$$\frac{d\rho}{dt} = A\frac{exp\left(-\frac{Q}{RT}\right)}{T}\frac{f(\rho)}{d^n} \tag{9}$$

$$A = \frac{C\gamma V^{\frac{2}{3}}}{R} \tag{10}$$

here, $\frac{d\rho}{dt}$ is the instantaneous rate of densification, d is the grain size, γ is the surface energy, V is the molar volume, R is the gas constant, T is the absolute temperature, Q is the activation energy, and $f(\rho)$ is a function only of density, and C is a constant.

The apparent activation energy, *Q*, is determined using natural logs to put equation (8) in the more general form, *y=mx+b*. It is possible then to construct an Arrhenius plot of $\ln\left(T\,\frac{dT}{dt}\frac{d\rho}{dT}\right)$ versus 1/T of the variations of the constant rate sintering data and determine Q for a specific sintered density ($f(\rho)$), following the assumption that the grain size is dependent only on the sintered density. This apparent activation energy for densification, at a given density, can then be determined from the slope (*m*) of a linear least squares fit to the sintering data, where *Q = -mR*. This relationship for the LTCC is shown in Figure #5 and for a submicrometer-sized calcined alumina (A16) (α-Al_2O_3, Alcoa Industrial Chemicals, Pittsburgh, PA), in Figure #6.

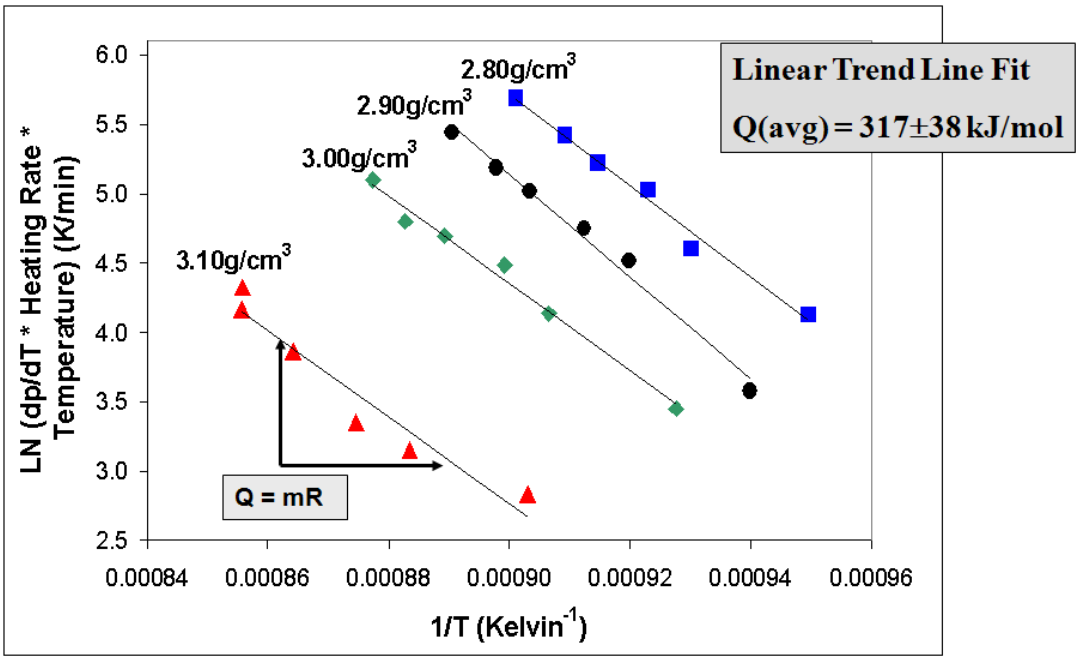

Figure #5. Arrhenius plot of $\ln\left(T\,\frac{dT}{dt}\frac{d\rho}{dT}\right)$ versus 1/T of the variations of the constant rate sintering data and determination of the Q for a specific sintered density ($f(\rho)$) for the Dupont low temperature co-fire dielectric tape, 951 Green Tape™.

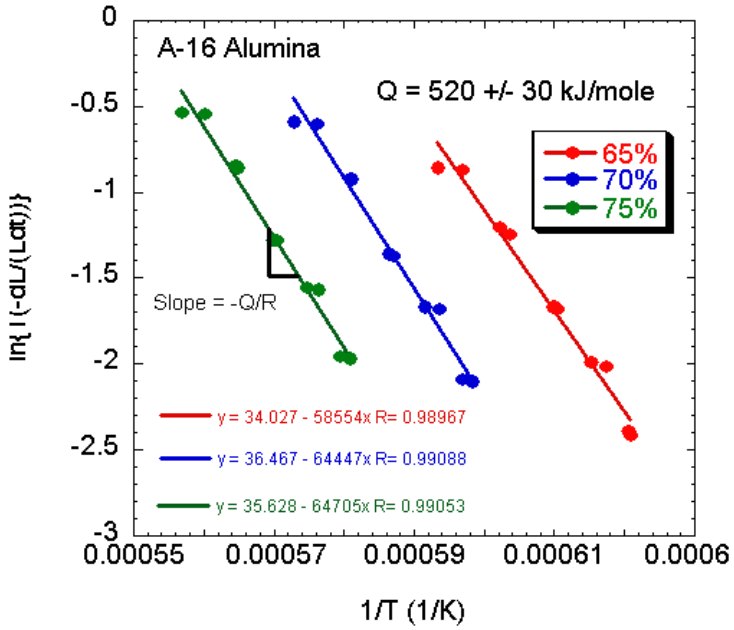

Figure #6. Arrhenius plot of $\ln\left(T\,\frac{dT}{dt}\frac{d\rho}{dT}\right)$ versus 1/T of the variations of the constant rate sintering data and determination of the Q for a specific sintered density ($f(\rho)$) for submicrometer-sized calcined alumina (A16) (α-Al_2O_3, Alcoa Industrial Chemicals, Pittsburgh, PA),

As long as the temperature as a function of time is known from the beginning to the end of the thermal profile, the master sintering curve can be generated from the measured and calculated densities as a function log θ(t, T(t)) (Note: it may be important to include the early stages of cooling if significant densification is still occurring). A master sintering curve was obtained for the 951 Green Tape™, and the apparent activation energy for sintering was determined to be approximately 346kJ/mol (317±38kJ/mol). The constructed master sintering curve for this system is shown in Figure #7.

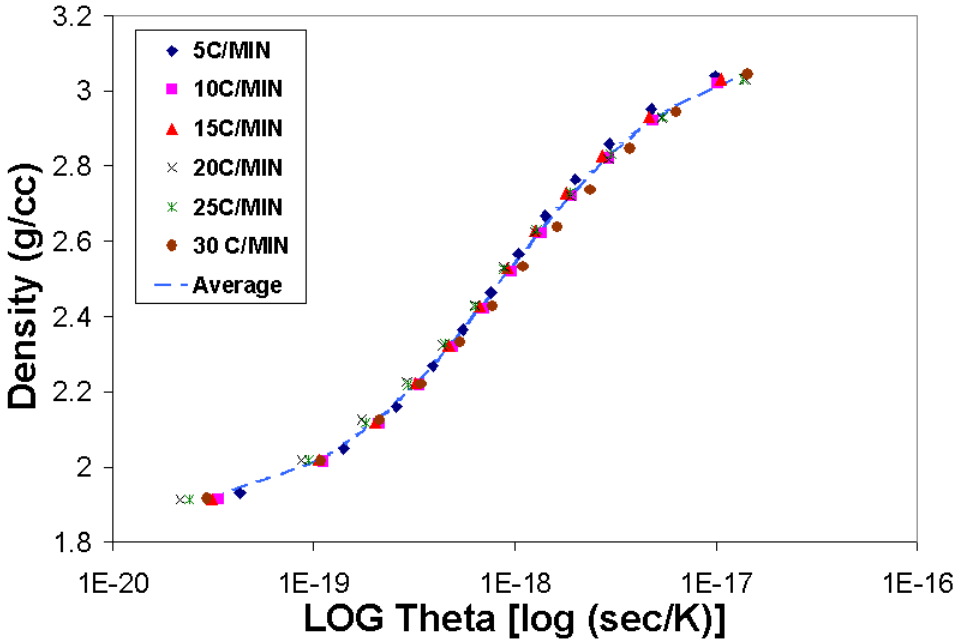

Figure #7. Master sintering curve for the Dupont low temperature co-fire dielectric tape, 951 Green Tape™.

The density for an arbitrary temperature-time excursion can now be predicted from the master sintering curve. The resultant master sintering curve not only characterizes the densification behavior of this LTCC material but it also provides a means to predict green tape density as a function of sintering time and temperature (Figure #8), and allows one to assess lot-to-lot (materials) and run-to-run (process) variability in LTCC manufacturing (Figure #9). Figure #8 shows a series of eleven separate and unique thermal profiles, independent of those thermal profiles used to construct the master sintering curve, that were used to sinter the LTCC material. It also shows how the resultant Archimedes determined density values compared to the predicted density from the master sintering curve. It is apparent from the graph in this figure that all final densities were predicted accurately, within experimental error, based on the constructed master sintering curve. The comparison of lot-to-lot variability, in the graph of Figure #9, is an example of how a master sintering curve can be utilized in product quality control/quality assurance where the densification behavior of three separate lots of LTCC material was compared against the predicted MSC values utilizing two separate thermal profiles.

Sample Set	Ramp (°C/min)	Temperature (°C)	Dwell Time
1	5	700	Air Quenched
2	10	750	Air Quenched
3	5	750	Air Quenched
4	25	800	Air Quenched
5	20	750	10min
6	15	800	Air Quenched
7	5	800	Air Quenched
8	5, 20	700, 800	5min, 5min
9	10	750	50min
10	25	800	20min
11	5	850	Air Quenched

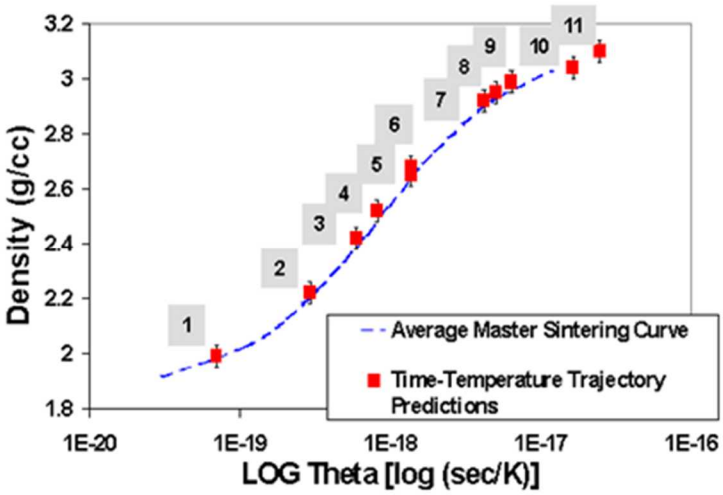

Figure #8. Density versus the master sintering curve parameter showing how eleven unique thermal profiles were predicted by the master sintering curve for the Dupont low temperature co-fire dielectric tape, 951 Green Tape™.

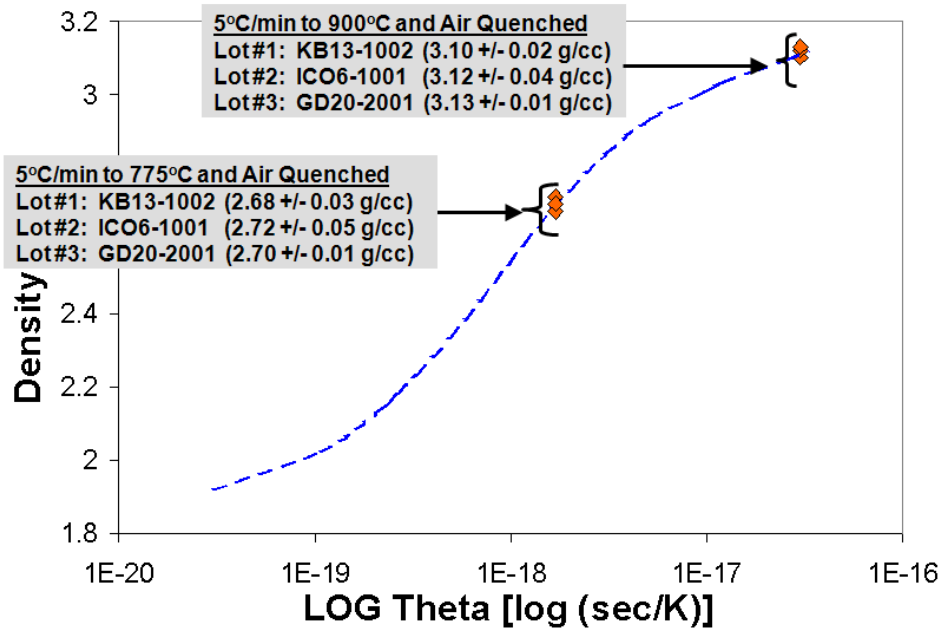

Figure #9. Density versus the master sintering curve parameter for Dupont low temperature co-fire dielectric tape, 951 Green Tape™, indicating how the master sintering curve can be utilized to assess lot-to-lot (materials) and run-to-run (process) variability in LTCC manufacturing.

It should also be noted that as useful as the concept of the mater sintering curve is, since certain conditions must be satisfied, not all sintering is expected to be described by a master sintering curve. The samples used to construct the curve must be consistent in powder characteristics, forming process, and overall green density. Also, under the conditions of interest, a 'single' or 'average' apparent activation energy must govern the sintering dynamics. In its purest form the master sintering curve has two critical assumptions imbedded in the theory. One, a single mechanism dominates densification and, two, G and Γ_b (the

microstructure evolution) are dependent only on density. It will be observable in the master sintering curve results if deviations from a single dominant diffusion mechanism with a single apparent activation energy exist. For example, a mechanism such as surface diffusion could result in extensive microstructure coarsening and consumption of the sintering driving force without any significant densification of the body. The coarsening due to surface diffusion, at the cost of densification, may be anticipated for slower heating rates and at lower densities, particularly during the initial sintering stage. This would be evidenced however by a change in the master sintering curve parameter and a possible change in the apparent activation energy for densification.

EXTENDING THE MASTER SINTERING CURVE TO THE THIRD DIMENSION

The concept of the master sintering curve, due to the intimate link established between ceramic processing, density, microstructure and the master sintering curve parameter, θ, can be taken a step further. It is possible to generate what can be referred to as 'master sintering curve surfaces' or 'master processing optimization maps' by effectively incorporating the materials property or parameter of interest, based on the intended application or a specific processing feature, as an additional variable in the construction of the master sintering curve. The MSC could be extended into the third dimension of, for example, green density or hot pressing pressure.[51] Figure #10 provides SEM images of the microstructure variation as a function of the final density, for the LTCC system, based on thermal profiles along the master sintering curve trajectory. It is at least qualitatively apparent from these images of the development of the microstructure as a function of density and the thermal profile as linked through the master sintering curve parameter. Thus if a specific and tailored microstructure is crucial to obtain a desired property or behavior for a particular electronic ceramic application, as is often the case, a 'master processing optimization map' would be highly desirable. This is generically shown in Figure #11.

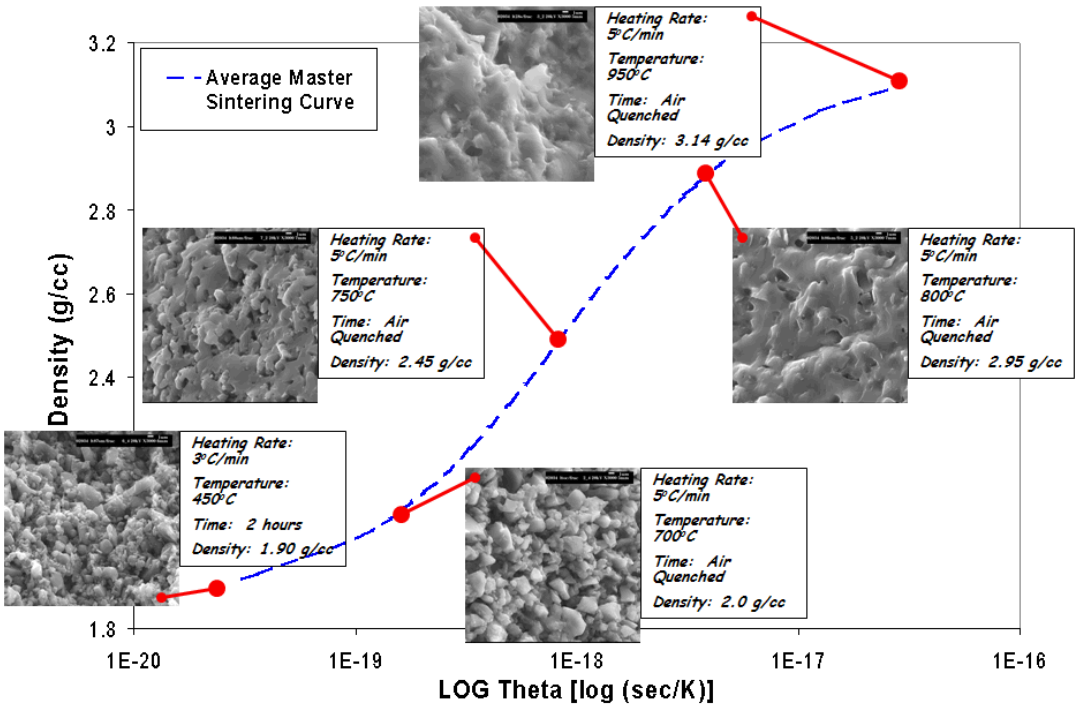

Figure #10. Qualitative microstructure trajectory as a function of the density and the master sintering curve parameter, based on a specific thermal profile, for the Dupont low temperature co-fire dielectric tape, 951 Green Tape™.

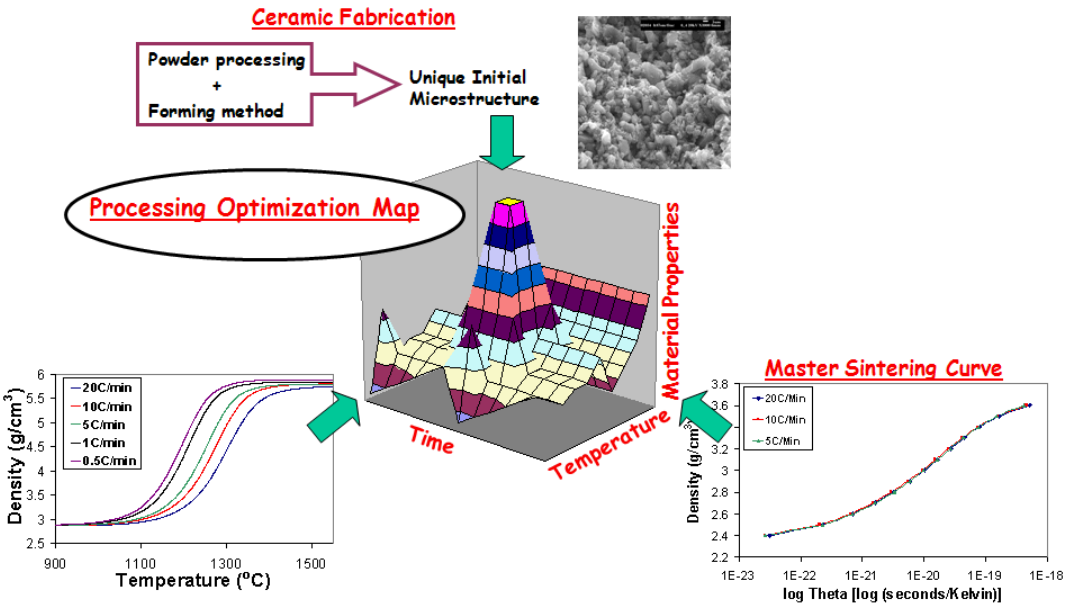

Figure #11. Generic representation of extending the mastering sintering curve into a third dimension and constructing 'master sintering curve surfaces' or 'master processing optimization maps'.

CASE STUDY: Controlling Electrical Performance of ZnO Varistors Using a Master Sintering Curve

Background

The nonohmic ZnO based ceramics have been widely used as varistors for voltage stabilization and transient surge suppression in electronic circuits and electric power systems since the late 1960's. This type of varistor is a ceramic semiconductor based on zinc oxide, ZnO, and various dopant elements resulting in a component having a highly nonlinear current-voltage relationship.[52,53] The electrical characteristics of ZnO varistor materials are determined by their detailed microstructure where three main microstructural features are especially important for determining their performance:

1. ZnO grain size, grain size distribution, and morphology
2. Grain boundary character
3. Intergranular network of bismuth rich phases

These features constitute the *functional microstructure* which is a result of the synthesis and forming techniques used for component fabrication and develops into maturity during sintering and densification. This case study was concerned with investigating the development of this functional microstructure and how, through implementation of the master sintering curve, a link could be established from synthesis and forming through sintering to final electrical performance. The objective then was to be able to predict and control the electrical performance of a ZnO varistor material through the construction and implementation of a master sintering curve and to establish a link between processing, sintering, microstructure and the macroscopic electrical behavior (current-voltage relationship).

Functional Microstructure

As for most ZnO varistor compositions, the composition used in this study, as listed in Table III, resulted in a microstructure containing ZnO grains, zinc silicate grains, spinel grains, and various bismuth-rich phases, as revealed through x-ray diffraction and SEM-EDS spectral mapping analysis and shown in Figure #12.

Table III. Additives and dopants used in this ZnO-based varistor composition for tailoring the microstructure and the component electrical behavior.

Material	*Compositional Role*	*Mol%*	*Weight%*
ZnO	Conductive Grains	81.45	82.61
Bi_2O_3	Non-Linearity Inducer	2.43	0.43
CoO	Non-Linearity Enhancer	0.87	0.43
MnO_2	Non-Linearity Enhancer	0.45	0.43
Sb_2O_3	Non-Linearity Enhancer	3.04	1.01
Cr_2O_3	Non-Linearity Enhancer	0.79	0.43
SiO_2	Grain Growth Retardant	9.84	13.51
NiO	Stability Enhancer	0.78	0.86
H_3BO_3	Stability Enhancer	0.13	0.17
$BaCO_3$	Stability Enhancer	0.21	0.09
Al	ZnO Conductivity Enhancer	0.01	0.03

(A)

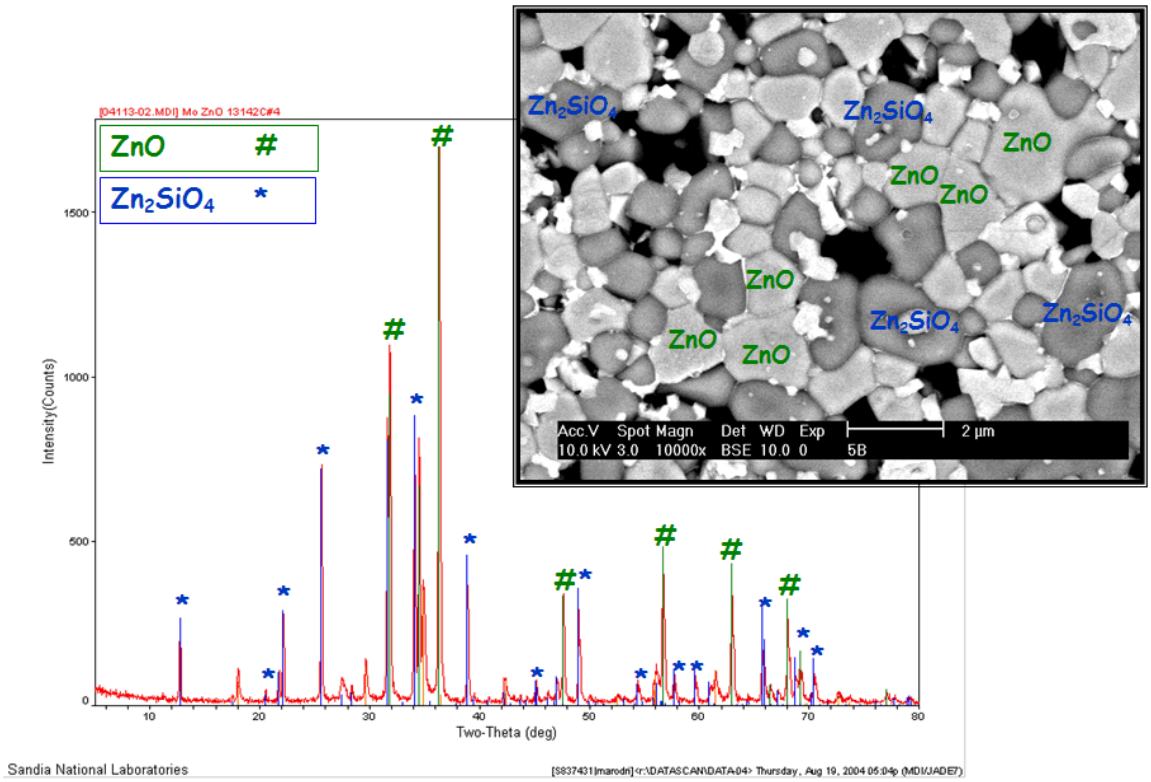

(B)

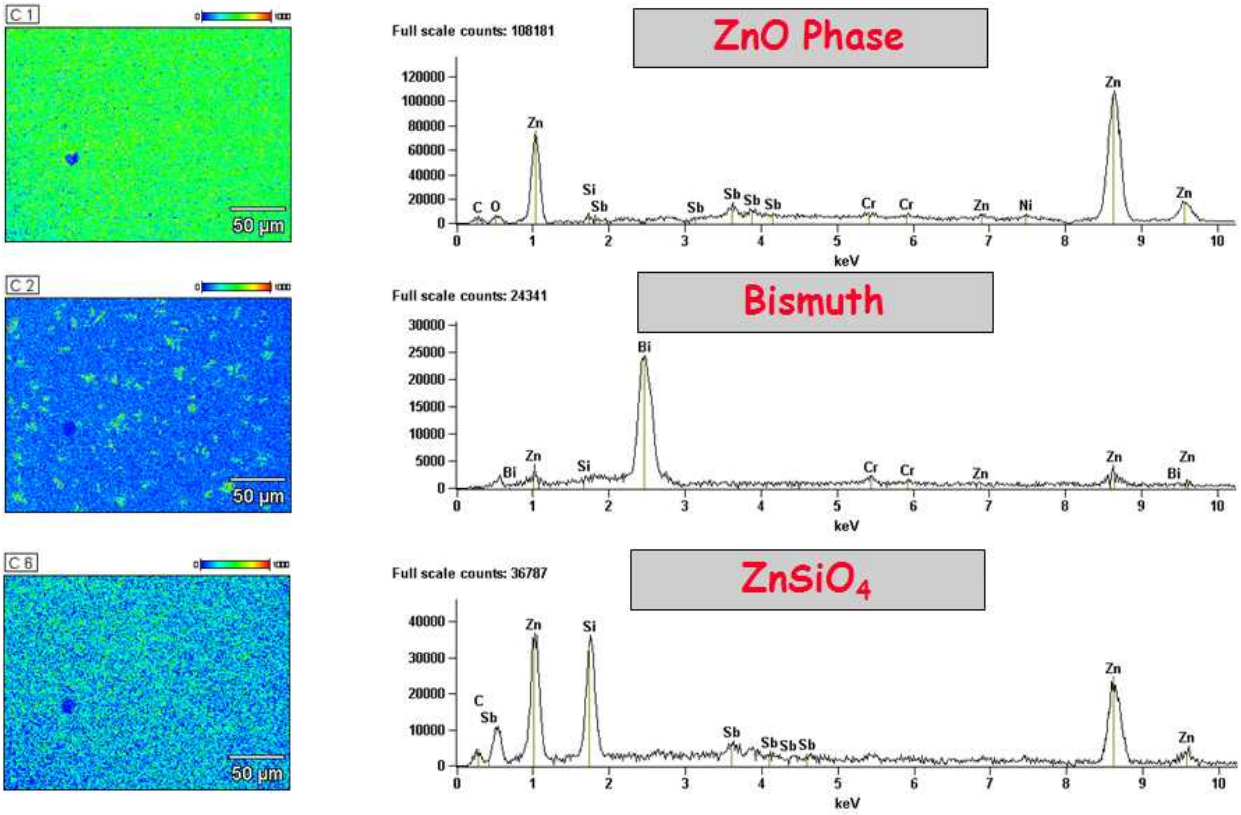

Figure #12. (A) Powder X-ray diffraction and (B) SEM-EDS spectral mapping analysis of ZnO varistor material revealing the two major phases of ZnO and $ZnSiO_4$ and the intergranular bismuth network.

In this case the spinel grains are considered electrically insulating and do not directly contribute to the electrical characteristics. The microstructural components that have a direct influence on the electrical characteristics[52,53], or the functional microstructure, consist of:

1. Doped ZnO grains – responsible for the conductivity in the material, especially in the 'up-turn' region of the current-voltage behavior.
2. Interfaces between the ZnO grains – provide barriers to electrical conduction, produce the nonlinear properties.
    a. The breakdown voltage of each individual interface depends on the microstructure of that interface.
    b. The electrical characteristics are based on the type of interfaces and the grain size (grain size distribution) as this determines the number of barriers to conduction.
3. Three-dimensional network of bismuth rich phases – located along the multiple ZnO grain junctions (triple junctions and their intersections at quadruple points).
    a. The bismuth rich phases form a network that contributes an additional current path.
    b. This path circumvents the barriers at the ZnO grain interfaces and can give a significant contribution to the conductivity in the pre-breakdown region where the network conductivity is determined by its internal microstructure.

The samples prepared for this case study were dry pressed discs that all had a similar initial microstructure and an 'as-pressed' density of 2.85±0.02g/cm^3. A series of sintering/densification curves were constructed from the dilatometric characterization of the samples displacement behavior as a function of constant heating rate experiments at 1, 3, 5, 10, 15 and 20^{o}C/min. The constructed densification curves as a function of temperature for each constant heating rate are shown in the plot in Figure #13.

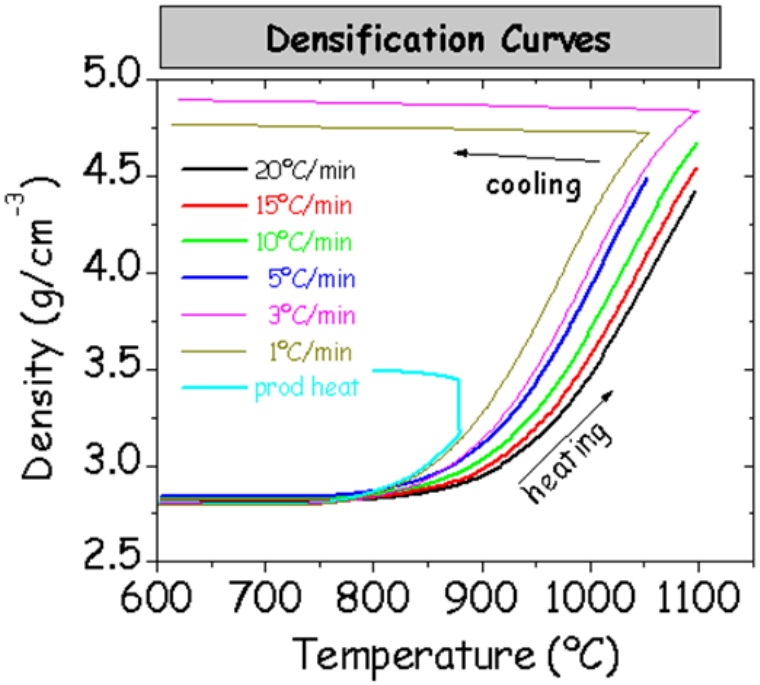

Figure #13. The constructed densification curves as a function of temperature for 1, 3, 5, 10, 15, and 20°C/min constant heating rates for the ZnO-based varistor composition samples.

The characterization results of the dilatometric behavior of the samples and the constructed densification curves were used to build a master sintering curve and determine an apparent activation energy for this ZnO varistor composition sintered under these conditions, the results of which are shown in Figure #14. An apparent activation energy was determined to be ~394 kJ/mole from the mean square residuals fit of the data (Figure #14 inset).

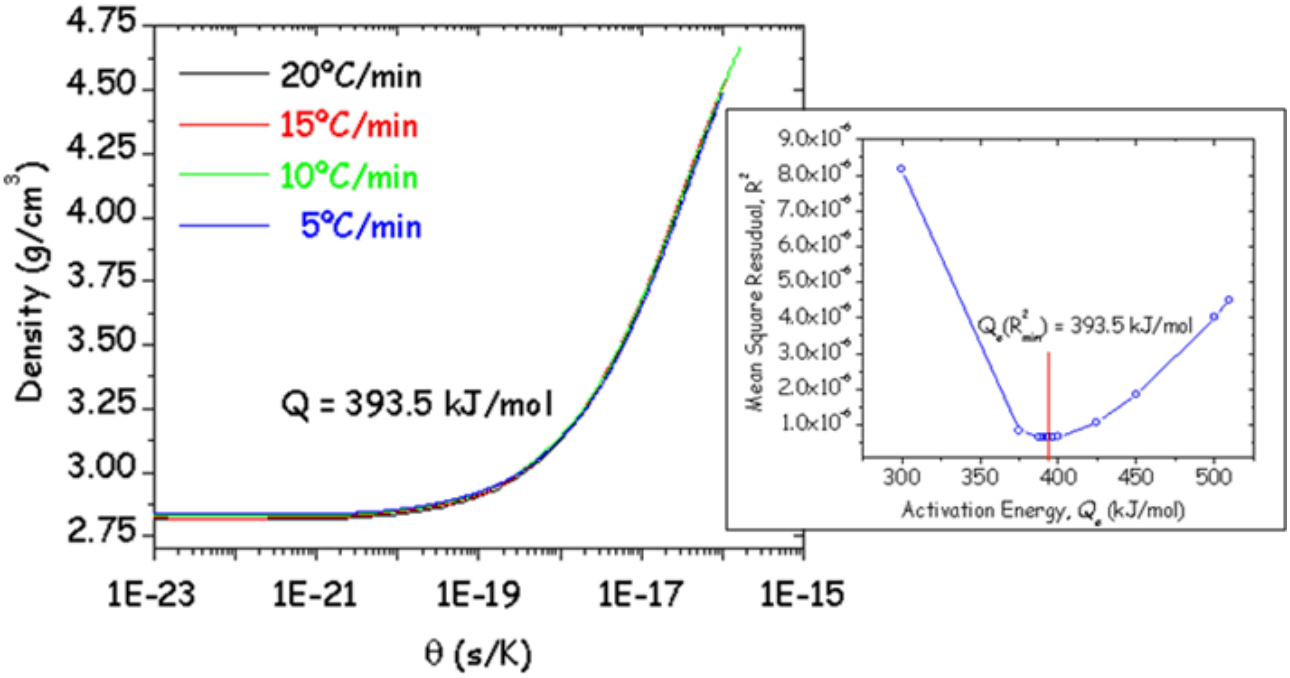

Figure #14. The constructed master sintering curve for a ZnO based varistor composition using 5, 10, 15, and 20°C/min constant heating rate dilatometer results. (Inset shows the mean square residual analysis performed to estimate the apparent activation energy for sintering).

Based on these results and the development of a master sintering curve for this system three distinct thermal profiles were chosen to verify and establish the link between the matured functional microstructure, the master sintering curve parameter and the electrical behavior of the material based on the functional microstructure. The goal being to prove the underlying hypothesis that the electrical behavior of the material, voltage-current relationship in the 'pre-breakdown' and 'breakdown' region, is a direct function of the final functional microstructure as predicted through the master sintering curve parameter. The three sample sets, the chosen thermal profiles, percent of theoretical density of the 'as-sintered' samples, and average grain size information and representative SEM images of the microstructure for each sample set (SS#1 – sample set #1, SS#2 – sample set #2, and SS#3 – sample set #3) is shown in Figure #15.

Sample Set	% of Theo. Density (g/cm^3) ($5.1 g/cm^3$)	Avg. ZnO Grain Intercept (ZnO/μm)	Avg. ZnO Grain Size(μm)	$ZnSiO_4$ Avg. Grain Intercept ($ZnSiO_4$/μm)	$ZnSiO_4$ Avg. Grain Size (μm)
SS #1 : 5°C/min to 950°C	69±1 (31% Porosity)	0.63±0.06	0.95±0.06	0.71±0.06	1.07±0.06
SS #2 : 20°C/min to 980°C	70.50±1 (28% Porosity)	0.61±0.05	0.92±0.05	0.69±0.06	1.04±0.06
SS #3 : 20°C/min to 1100°C	91.50±1 (8.5% Porosity)	0.92±0.04	1.38±0.04	0.89±0.06	1.34±0.06

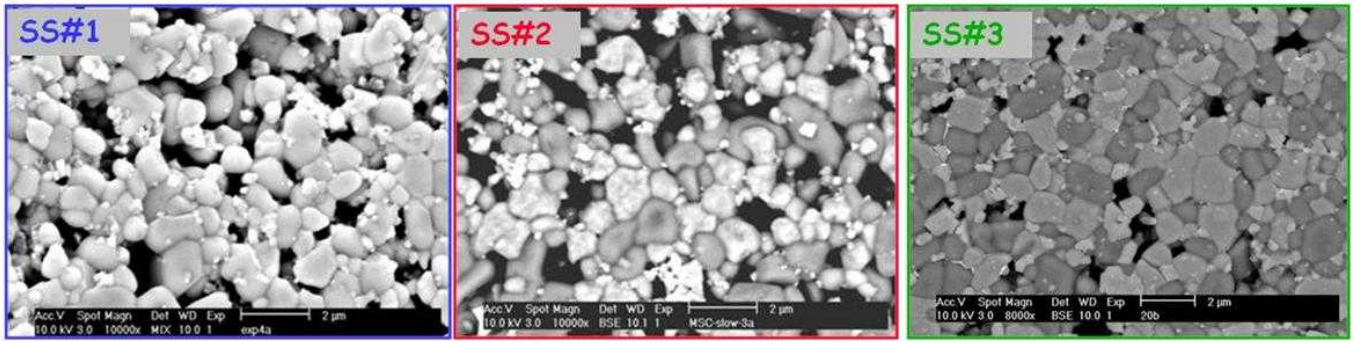

Figure #15. Information and results for the three sample sets chosen for linking the functional microstructure through the master sintering curve parameter to the electrical behavior (including; the thermal profiles, percent of theoretical density, and the average grain size results) and representative SEM images of the microstructure for each sample set (SS#1 – sample set #1, SS#2 – sample set #2, and SS#3 – sample set #3).

The thermal profiles for sample sets labeled SS#1 and SS#2 were each unique, however they were chosen based on the master sintering curve prediction to produce similar microstructures. The thermal profile for SS#3 was chosen to produce a distinctively different microstructure from SS#1 and SS#2. The results in Figure #15 verify that SS#1 and SS#2 have these similar characteristics and are unique from those determined for SS#3. Therefore, if the electrical behavior is intimately tied to the functional microstructure then SS#1 and SS#2 should have nearly identical electrical behavior and SS#3 should be unique. The electrical behavior for each sample set was characterized in the 'pre-breakdown' and 'breakdown' region for the voltage-current relationship. The results, from this analysis, are shown in Figure #16. It is apparent that the current-voltage behavior is nearly identical for SS#1 and SS#2, each having a breakdown voltage value of approximately 48kV/cm and an alpha value of approximately 19, and unique for SS#3, breakdown voltage of approximately 28kV/cm and an alpha value of approximately 21. These results establish and verify the link between the master sintering curve parameter, functional microstructure and electrical properties and thus demonstrate the ability to predict the electrical behavior from the master sintering curve.

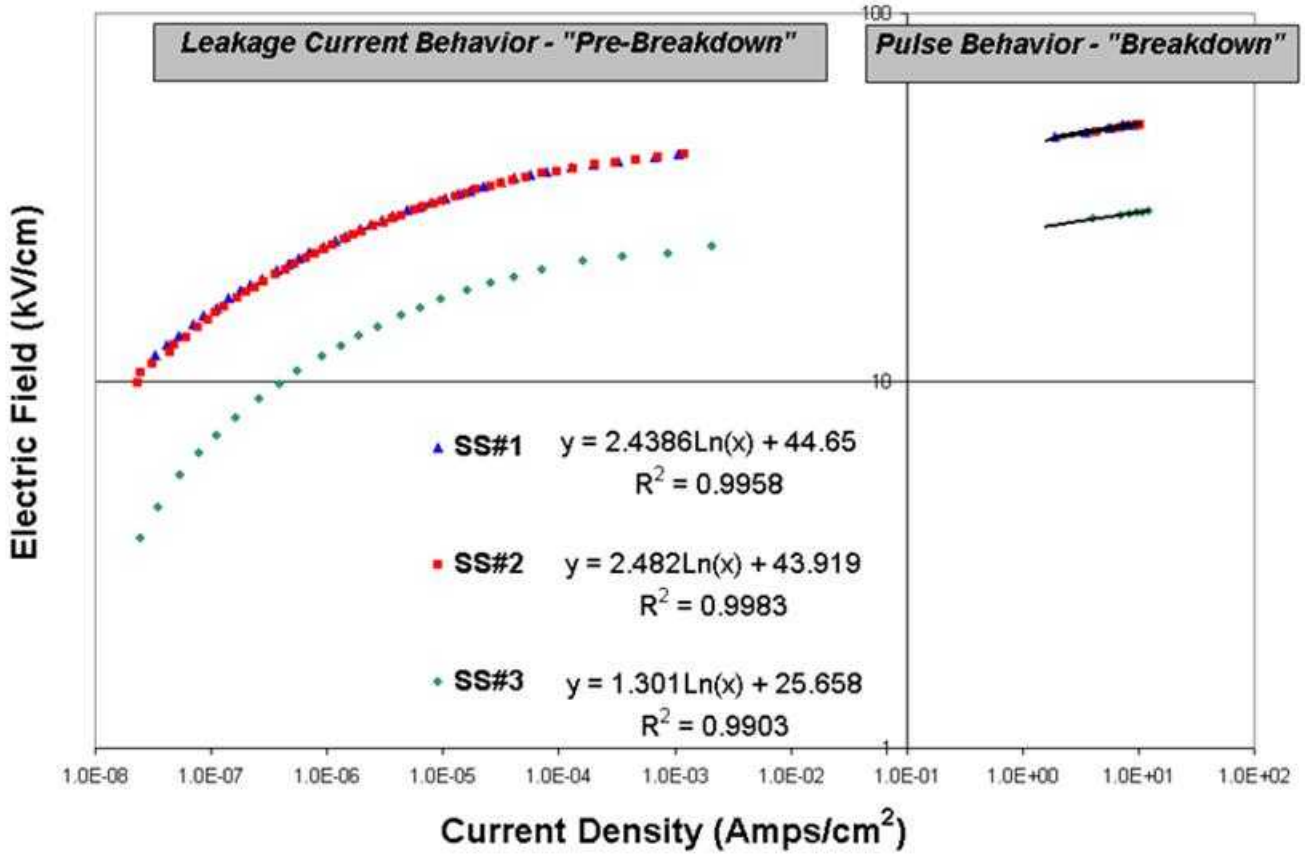

Sample Set	$E_{Breakdown}$ Breakdown Field @ 5 Amps/cm² (kV/cm)	Alpha (5-10 Amps/cm²)
SS #1 : 5°C/min to 950°C	47.90	19.30
SS #2 : 20°C/min to 980°C	48.57	19.90
SS #3 : 20°C/min to 1100°C	27.75	21.03

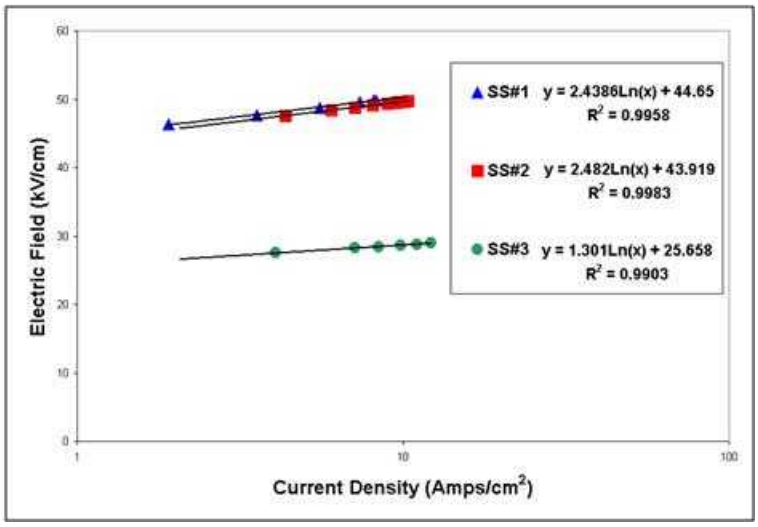

Figure #16. Electrical behavior results for the three sample sets chosen for linking the functional microstructure through the master sintering curve parameter to the electrical behavior (SS#1 – sample set #1, SS#2 – sample set #2, and SS#3 – sample set #3), including the calculated breakdown voltage and alpha values for each sample set.[52-53]

It has been shown, through this case study, that the detailed microstructure of the ZnO varistor material is strongly dependent upon the fabrication variables, in particular the sintering profile. The functional microstructure, established based on the sintering profile, directly influences the electrical properties of these materials. Therefore a process optimization map can be constructed through proper utilization of a master sintering curve, as depicted generically in the schematic in Figure #17.

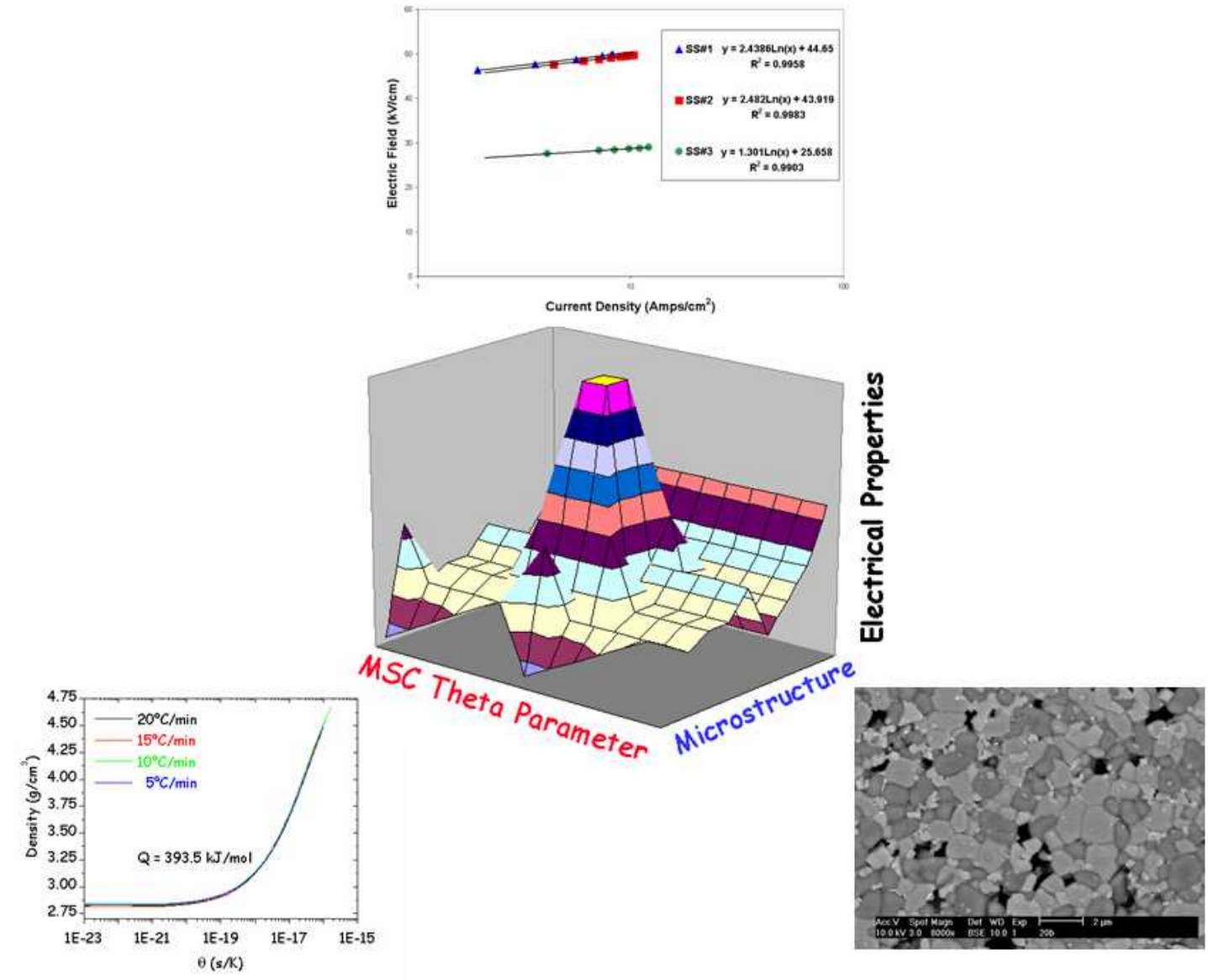

Figure #17. Generic processing optimization map constructed from establishing a link between the functional microstructure and the electrical behavior through the development of a master sintering curve for a ZnO varistor material.

CONCLUSION

For advanced ceramic component manufacturing, reproducible processing, sintering and densification of ceramic systems intended for application as electronic ceramics is critical for the cost-effective manufacture of reliable electronic ceramic components. Empirical engineering has historically been used to develop the techniques to manufacture these components. This alone however cannot provide the fundamental understanding necessary to design new electronic ceramic products, process new electronic ceramic materials and properly sinter and densify these materials to the desired requirements to produce components with the necessary electronic properties for a tailored application.

Master sintering curve theory, although a relatively young concept, can provide the electroceramist with a characteristic measure of the sinterability of a ceramic body. It results in a single empirical densification curve that is, by design, independent of the heating history. It takes advantage of the parameters used in the sintering rate equation by separating those relating microstructure and time-temperature terms to opposite sides of an empirical equation. The formulation and construction of the master sintering curve has its roots in and can be derived from the combined stage sintering model where the analysis of sintering has been extended beyond the segments described by the individual stage models that incorporate idealized geometric considerations that fail in properly representing the entire sintering process. A master sintering curve parameter and the equations used in construction of the curve are then developed through a subsequent rearrangement of this combined stage sintering model and are governed by a series of assumptions. The first being that a single dominant diffusion mechanism exists in a system where grain boundary or volume diffusion dominates the sintering process. Although a master sintering curve may not be entirely applicable in systems where surface or vapor transport are the active and dominate diffusion mechanisms or in cases of exaggerated grain growth, it can indicate the presence of these factors. Second, the master sintering curve is a single valued function of density where the mean grain diameter and scaling parameters are only a function of the density of the material and not the time-temperature profile. Therefore, for a given powder system, green microstructure and green density the developed mastering sintering curve would be considered unique. The constructed master sintering curve would be ultimately modified if any changes were made to the green microstructure by variations in the particle size distribution, average particle size, initial pore-size distribution, and particle packing properties. Under these assumptions and after some mathematical manipulation of the combined stage sintering equation the master sintering curve is developed through the underlying relation, $\Phi(\rho) \equiv \theta(t, T(t))$.

The ability to predict and control sintering and densification from master sintering curve theory and ultimately link this to the ceramic processing, microstructure development and electronic properties provides the practical value from the concept and its use. This allows for the integration of fundamental scientific understanding into science-based processing technology to gain a better understanding and control over ceramic powder processing and sintering. Master sintering curve theory has been successfully applied to the sintering of numerous ceramic systems. The findings presented here demonstrate that a systematic approach to design, predict and control sintering of electroceramic systems is possible through the implementation of the master sintering curve.

ACKNOWLEDGEMENTS

The authors would like to sincerely thank I. Nettleship and T. Chen, University of Pittsburgh, Pittsburgh, PA, for contributions and discussions on the microstructure analysis for the ZnO varistor material and Alex Roesler, Sandia National Laboratories, Albuquerque, NM, for a critical review of the chapter contents.

REFERENCES

1. W. D. Kingery, H. K. Bowen, and D. R. Uhlmann, *Introduction to Ceramics*, 2nd Edition, (1976), Wiley, New York.

2. A. J. Moulson and J. M. Herbert, *Electroceramics: Materials, Properties, Applications*, 2nd Edition, (2003), John Wiley and Sons, Ltd.

3. R. L. Coble and J. E. Burke, "*Sintering in Ceramics*," in Progress in Ceramic Science, Volume 3, Edited by J. E. Burke, The MacMillan Company, New York, 1963, pp. 197-251.

4. F. Thümmler and W. Thomma, "*The Sintering Process*," *J. Inst. Metals* **12**, 69-108 (1967).

5. J. E. Burke and J. H. Rosolowski, "*Sintering," in Treatise on Solid State Chemistry, Volume 4, Reactivity of Solids*, Edited by N. B. Hannay, Plenum Press, New York, 1976, pp. 621-59.

6. R. L. Coble, ‘‘*Sintering of Crystalline Solids I: Intermediate and Final Stage Diffusion Models*,’’ J. Appl. Phys., 32 [5] 787–92 (1961).

7. R. M. German, *Liquid Phase Sintering*, Plenum Press, New York, 1985.

8. C. J. Brinker and G. W. Scherer, *Sol-Gel Science, The Physics and Chemistry of Sol-Gel Processing*, Academic Press, Inc., New York, 1990, pp. 675-742.

9. K. G. Ewsuk, “*Consolidation of Bulk Ceramics*” in Characterization of Ceramics, edited by R. E. Loehman, Butterworth-Heinemann, Greenwich, CT, 1993, pp.77-101.

10. J. S. Reed, *Introduction to the Principles of Ceramic Processing*, second edition, John Wiley & Sons, Inc., New York, 1995, pp. 583-619.

11. K. G. Ewsuk, “*Ceramics (Processing)*,” in the Kirk-Othmer Encyclopedia of Chemical Technology, Fourth Ed., Vol. 5, John Wiley & Sons, Inc., New York, NY, 1993, pp.620-627.

12. D. W. Richerson, *Modern Ceramic Engineering: Properties, Processing, and Use in Design*, second edition, Marcel Dekker, Inc., New York, 1992, pp. 519-564.

13. C. Herring, “*Surface Tension as a Motivation for Sintering*,” pp. 143-179 in The Physics of Powder Metallurgy, edited by W. E. Kingston, McGraw-Hill Book Company, Inc., New York, (1949).

14. W. D. Kingery and B. Francois, "*The Sintering of Crystalline Oxides, I. Interactions Between Grains Boundaries and Pores*," in Sintering and Related Phenomena, edited by G. C. Kuczynski, N. A. Hooton, and C. F. Gibbon, Gordon and Breach Science Publishers, New York, 1965, pp 471-498.

15. K. G. Ewsuk, *Final Stage Densification of Alumina During Hot Isostatic Pressing*, Ph. D. Thesis, The Pennsylvania State University, 1986.

16. K. G. Ewsuk and G. L. Messing, "*A Theoretical and Experimental Analysis of Final-Stage Densification of Alumina During Hot Isostatic Pressing*," in Hot Isostatic Pressing: Theories and Applications, edited by R. J. Schaefer and M. Linzer, ASM International, Materials Park OH, 1991, pp. 23-33.

17. K. G. Ewsuk, ‘‘*Ceramic Processing*”; pp. 2457–72 in Encyclopedia of Chemical Physics and Physical Chemistry, Vol. III, Applications, Edited by J. H. Moore and N. D. Spencer. IOP Publishing Ltd, Philadelphia, 2001.

18. K. G. Ewsuk, J. Arguello, and D. Zeuch, ‘‘*Characterizing and Predicting Density Gradients in Particulate Ceramic Bodies Formed by Powder Pressing*’’; pp. 169–76 in Proceedings of the Green Body Characterization Symposium, German Ceramic Society, 2001.

19. K. G. Ewsuk and J. G. Arguello, ‘‘*Controlling Processing Through Science-Based Understanding and Modeling*’’; pp. 169–78 in Proceedings of the 2nd International Conference on Shaping Advanced Ceramics, Edited by J. Luyten and J. P. Erauw, Flemish Institute for Technological Research (Vito), 2002.

20. K. G. Ewsuk and J. G. Arguello, ‘‘*Controlling Ceramic Powder Compaction Through Science-Based Understanding*,’’ Key Eng. Mater., 264–268, 149–54 (2004).

21. K. G. Ewsuk and J. G. Arguello, ‘‘*Science Based Ceramic Powder Processing*,’’ Key Eng. Mater., 247, 27–34 (2003).

22. K. G. Ewsuk, J. Arguello, D. Zeuch, B. Farber, L. Carinci, J. Kaniuk, J. Keller, C. Cloutier, B. Gold, R. Cass, J. French, B. Dinger, and W. Blumenthal, ‘‘*CRADA Develops Model for Powder Pressing and Die Design, Part 1*,’’ Bull. Am. Ceram.Soc., 80 [1] 53–60 (2001).

23. K. G. Ewsuk, J. Arguello, D. Zeuch, B. Farber, L. Carinci, J. Kaniuk, J. Keller, C. Cloutier, B. Gold, R. Cass, J. French, B. Dinger, and W. Blumenthal, ‘‘*CRADA Develops Model for Powder Pressing and Die Design, Part 2*,’’ Bull. Am. Ceram. Soc., 80 [2] 41–6 (2001).

24. K. G. Ewsuk, J. G. Arguello, D. N. Bencoe, D. T. Ellerby, S. J. Glass, D. H. Zeuch, and J. A. Anderson, ‘‘*Characterizing Powders for Dry Pressing, Sintering*,’’ Bull. Am. Ceram. Soc., 82 [5] 41–7 (2003).

25. W. D. Kingery and B. Francois, ‘‘*The Sintering of Crystalline Oxides I, Interactions Between Grain Boundaries and Pores*’’; pp. 471–96 in Sintering and Related Phenomena, Edited by W. D. Kingery, N. A. Hooten, and C. F. Gibbon, Gordon and Breach Science Publishers, New York, 1967.

26. J. E. Burke and J. H. Rosolowski, ‘‘*Sintering*”; pp. 621–59 in Reactivity of Solids, Treatise on Solid State Chemistry (Chapter 10), Vol. 4, Edited by N. B. Hannay, Plenum Press, New York, 1976.

27. J. Hansen, R. P. Rusin, M. Teng, and D. L. Johnson, ‘‘*Combined-Stage Sintering Model*,’’ J. Am. Ceram. Soc., 75 [5] 1129–35 (1992).

28. M. F. Ashby, ‘‘*A First Report on Sintering Diagrams*,’’ Acta Metall., 22 [3] 275–89 (1974).

29. J. Zhao and M. Harmer, ‘‘*Effect of Pore Distribution on Microstructure Development: II, First and Second Generation Pores*,’’ J. Am. Ceram. Soc, 71 [7] 530–9 (1988).

30. E. Artz, M. F. Ashby, and K. E. Easterling, ‘‘*Practical Applications of Hot-Isostatic Pressing Diagrams: Four Case Studies*,’’ Metall. Trans. A., 14A, 211–21 (1983).

31. D. S. Wilkenson and M. F. Ashby, ‘‘*The Development of Pressure Sintering Maps*’’; pp. 473–92 in Sintering and Catalysis, Materials Science Research, Vol. 10, Edited by G. C. Kuczinski, Plenum Press, New York, (1975).

32. F. B. Swinkels and M. F. Ashby, ‘‘*A Second Report on Sintering Diagrams*,’’ Acta. Metall., 29, 259–81 (1981).

33. M. P. Harmer, ‘‘*Use of Solid-Solution Additives in Ceramic Processing*’’; pp. 679–96 in Structure and Properties of MgO and Al_2O_3 Ceramics, Advances in Ceramics, Vol. 10, Edited by W. D. Kingery, The American Ceramic Society, Columbus, OH, 1984.

34. K. G. Ewsuk, ‘‘*Sintering Maps for Ceramic-Filled-Glass Composites,*’’; pp. 125–35 in Ceramic Transactions, Vol. 19, Advanced Composite Materials: Processing, Microstructure, Bulk and Interfacial Characterization, Characterization Methods and Applications, Edited by M. D. Sacks, The American Ceramic Society, Westerville, OH, 1991.

35. H. Su and D. L. Johnson, ''*Master Sintering Curve, A Practical Approach to Sintering*,'' J. Am. Ceram. Soc., 79 [12] 3211–7 (1996).

36. C. B. DiAntonio and K. G. Ewsuk, ''*Controlled and Predicted Ceramic Sintering Through Master Sintering Curve Theory*,''; pp. 15–23 in Ceramic Transactions, Vol. 157, Edited by C. B. DiAntonio, The American Ceramic Society, Westerville, OH, 2004.

37. C. B. DiAntonio, D. N. Bencoe, and K. G. Ewsuk, ''*Characterization and Control of Low Temperature Co-Fire Ceramic (LTCC) Sintering*,'' Proc. Soc Photo-Optical Instr. Eng. (SPIE), 5231, 160–4 (2003).

38. K. G. Ewsuk, C. B. DiAntonio, F. Uribe, and S. Monroe, ''*Materials and Process Control Technology for LTCC Microelectronics Packaging,*''; pp. 1–6 in Proceedings of the Ceramic Interconnect Technology. The Next Generation II, International Microelectronics and Packaging Society, Washington, DC, 2004.

39. D. Li, S.O. Chen, X. Q. Sun, W. Q. Shao, Y. C. Zhang, and S. S. Zhang, "*Construction and validation of master sintering curve for TiO_2 for pressureless sintering*," Advances in Applied Ceramics, 2008, vol. 107, no. 1, pp. 52-56.

40. D. L. Johnson, ''*Finding and Utilizing the Master Sintering Curve*''; pp. 15–7, Sintering 2003, International Conference on the Science, Technology, Application of Sintering, September 2003.

41. C. B. DiAntonio, K. G. Ewsuk, and D. N. Bencoe, ''*Control of Low Temperature Co-Fire Ceramic Sintering*''; pp. 15–7, Sintering 2003, International Conference on the Science, Technology, and Application of Sintering, September 2003.

42. D. C. Blaine, S. Park, and R. M. German, ''*Master Sintering Curve for a Two-Phase Material*''; pp. 264–7, Sintering 05, 4th International Conference on Science, Technology, and Application of Sintering, August–September 2005.

43. K. An and M. K. Han, ''*Microstructural Evolution Based on the Pressure-Assisted Master Sintering Surface*,'' Mater. Sci. Eng. A, 391, 66–70 (2005).

44. T. R. G. Kutty, K. B. Khan, P. V. Hegde, J. Banerjee, A. K. Sengupta, S. Majumdar, and H. S. Kamath, ''*Development of a Master Sintering Curve for ThO_2*,'' J. Nucl. Mater., 327, 211–9 (2004).

45. M. H. Teng, Y. Lai, and Y. Chen, ‘‘*A Computer Program of Master Sintering Curve Model to Accurately Predict Sintering Results*,’’ West. Pacific Earth Sci., 2, 2171–80 (2002).

46. S. Kiani, J. Pan, J. A. Yeomans, “*A New Scheme of Finding the Master Sintering Curve*,” J. Am. Ceram. Soc., 89 [11] 3393–3396 (2006).

47. K. G. Ewsuk, D. T. Ellerby, and C. B. DiAntonio, “*Analysis of Nanocrystalline and Microcrystalline ZnO Sintering Using Master Sintering Curves*,” J. Am. Ceram. Soc., 89 [6] 2003–2009 (2006).

48. R. T. DeHoff, “*A Cell Model for Microstructural Evolution during Sintering*,” in Materials Science Research, Vol. 16, *Sintering and Heterogeneous Catalysis*, Edited by G. C. Kuczynski, A. E. Miller, and G. A. Sargent, Plenum Press, New York, (1984), pp. 23-34.

49. W. S. Young and I. B. Cutler, ‘‘*Initial Sintering with Constant Rates of Heating*,’’ J. Am. Ceram. Soc., 53 [12] 659–63 (1970).

50. J. Wang and R. Raj, ‘‘*Estimate of the Activation Energies for Boundary Diffusion from Rate-Controlled Sintering of Pure Alumina, and Alumina Doped with Zirconia or Titania*,’’ J. Am. Ceram. Soc., 73 [5] 1172–5 (1990).

51. K. An and D. L. Johnson, “*The pressure-assisted master sintering surface*,” J. Materials Science, 37 (2002) 4555-4559.

52. L. M. Levinson and H. R. Philipp, “*The Physics of Metal Oxide Varistors*,” Journal of Applied Physics, Volume 46, No. 3, March 1975, pp. 1332-1341.

53. D. R. Clarke, “*Varistor Ceramics*,” Journal of the American Ceramic Society, Volume 82, Issue 3, pp. 485-502.